Journal of Catalysis 421 (2023) 285–299

Contents lists available at ScienceDirect

Journal of Catalysis

journal homepage: www.elsevier.com/locate/jcat

States of Pt/CeO_2 catalysts for CO oxidation below room temperature

Elena M. Slavinskaya [a,1], Andrey I. Stadnichenko [a,1], Jon E. Quinlivan Domínguez [b,1], Olga A. Stonkus [a], Mykhailo Vorokhta [c], Břetislav Šmíd [c], Pablo Castro-Latorre [b], Albert Bruix [b,*], Konstantin M. Neyman [b,d], Andrei I. Boronin [a,*]

[a] Boreskov Institute of Catalysis SB RAS, Pr. Ak. Lavrentieva 5, 630090 Novosibirsk, Russia
[b] Departament de Ciència de Materials i Química Física & Institut de Quimica Teòrica i Computacional (IQTCUB), Universitat de Barcelona, c/Martí i Franquès 1, 08028 Barcelona, Spain
[c] Department of Surface and Plasma Science, Faculty of Mathematics and Physics, Charles University, V Holešovičkách 2, 180 00, Prague 8, Czech Republic
[d] ICREA (Institució Catalana de Recerca i Estudis Avançats), 08010 Barcelona, Spain

ARTICLE INFO

Article history:
Received 21 October 2022
Revised 27 February 2023
Accepted 1 March 2023
Available online 6 March 2023

Keywords:
Pt/CeO_2
low-temperature CO oxidation
PtO_x clusters
Single atom

ABSTRACT

CO molecules can be efficiently oxidized over Pt/CeO_2 catalysts, but the stability and reactivity of different states of Pt in the catalysts are still unclear. Here we combine experimental and computational methods to characterize Pt/CeO_2 catalysts subjected to reductive and oxidative pre-treatments and exposed to CO oxidation reaction conditions. Particles of metallic Pt, known to be catalytically active at elevated temperature, are shown to be precursors for the formation, under *operando* conditions, of more stable PtO_x particles that enable CO oxidation below room temperature. These PtO_x particles are similarly stable to – but more active than – atomically dispersed Pt^{2+} species. The results and approaches presented in this study illustrate the complex response of catalytic materials to reaction conditions and pave the way for future efforts to improve Pt/CeO_2 and similar catalysts using dedicated pre-treatment strategies.

1. Introduction

Efficient oxidation of CO by catalysts at room and lower temperatures is indispensable, e.g. for solving the challenge of purifying indoor air and exhaust gases of vehicles in cold environments. Among the catalysts active toward CO oxidation at such low temperatures are those based on Co_3O_4 [1–3] and on oxide-supported noble metals Ir [4], Au [5–7], Pt [8–10], and Pd [11]. The catalytic activity and stability of supported noble metals in such materials are strongly affected by the metal-support interactions and by the nuclearity and oxidation state of the metal species. Pt/CeO_2 is one of the most stable systems, where Pt can form different oxidation states of both particles and single-atoms (Pt-SA), anchored to the CeO_2 support by strong Pt-O-Ce bonds. This strong interaction prevents aggregation and maintains high Pt dispersion even at elevated temperatures [12–15]. It is however one of the reasons for the relatively low activity of the Pt-SA sites in oxygen-rich environments, which over-stabilize Pt atoms. In turn, oxidation of Pt forming sub-nanometer PtO_x clusters on CeO_2 substantially enhances the low-temperature activity of Pt/CeO_2 catalysts [16].

Pretreatments of Pt/CeO_2 catalysts and their exposure to reactants can modify the nuclearity and state of the Pt species. These transformations have been characterized in recent studies, but the debate on the identity and oxidation state of the sites active at low temperatures is still not settled. Pt/CeO_2 catalysts pre-oxidized at 800 °C exhibited a higher reduction temperature in the temperature-programmed reaction with hydrogen (TPR-H_2) than catalysts pre-oxidized at 500 °C [17], indicating that Pt-O-Ce bonds are strengthened and more resistant to reduction by H_2 in catalysts pre-oxidized at higher temperatures.

Several studies show that reductive treatments improve the low-temperature CO oxidative activity of Pt/CeO_2 catalysts with respect to the unreduced catalysts. For example, the activity of Pt/CeO_2 catalysts reductively treated in an enriched synthetic exhaust mixture, increased both for the oxidation of CO and hydrocarbons and for the reduction of NO [18]. An enhancement of the catalytic activity at near-room temperature after the treatment of the catalyst in CO at 275 °C was also observed by Pereira-Hernández et al. [19]. These authors attributed the enhanced activity to the restructuring of CeO_2, which increases its reducibility, and to the partial transformation of Pt-SA centers into metallic Pt particles. The activity at near-room temperature of the Pt/CeO_2 catalysts also depends on the reducing agent employed, increasing in the order $C_3H_6 < H_2 < CO$ [20,21]. According to Grunwaldt and coworkers [20,21], one of the key factors determining the maximum

* Corresponding authors.
E-mail addresses: abruix@ub.edu (A. Bruix), boronin@catalysis.ru (A.I. Boronin).
[1] These authors contributed equally to this work and should be considered as co-first authors.

https://doi.org/10.1016/j.jcat.2023.03.004
0021-9517/

CO oxidative activity is the formation of Pt particles with the optimal size of ca. 1.4 nm. This agrees with the findings by Ding et al. that only Pt particles (on oxide supports) are active toward CO oxidation, whereas Pt single atoms behave as spectators [22].

Improvements in catalytic activity caused by Pt/CeO_2 treatment in H_2 at 200–300 °C almost disappeared after a mild re-oxidation at room temperature [23]. Pereira-Hernández et al. suggested [24] that a highly active state of the catalyst is induced by transforming atomic Pt into sub-nanometer Pt particles during the reductive treatment. At low Pt loadings, such Pt particles transform back into the stable (and less active) Pt-SA state under oxidizing conditions. Reduction of Pt-SA in H_2 can also create partially reduced Pt species active at room temperature [8,25]. In the reaction medium, such species transform into a less active state below 100 °C and fully re-oxidize at 150 °C. A beneficial effect of the treatment by H_2 was also reported for a $Pt/Ce_{0.64}Zr_{0.16}Bi_{0.20}O_{1.90}$ catalyst with 10 wt% Pt mediating virtually complete CO conversion at 0 °C [10]. Unfortunately, that catalyst was not examined in several cycles of CO oxidation, which as we show in this work is crucial to understand the response of the catalyst to pre-treatments and reaction conditions. We note that although the content of Pt in the $Pt/Ce_{0.64}Zr_{0.16}Bi_{0.20}O_{1.90}$ catalyst was fourfold greater than that of the Pt/CeO_2 catalyst used in [8], the low-temperature performance of the higher-loaded catalyst exceeds that of the lower-loaded one in terms of specific activity (i.e. activity normalized by the platinum loading).

Despite the pre-treatment of Pt/CeO_2 catalysts in H_2, some studies report the presence *and* CO oxidative activity of partially oxidized Pt species [26–29]. According to Hong and Sun [27], Pt is initially present as slightly negatively charged species after reduction by H_2. However, the resulting increased activity of the reduced catalyst was attributed to its capacity to adsorb larger amounts of oxygen (and become more oxidized) than the unreduced catalyst. Qu and co-workers proposed that the thermal treatment by H_2 leads to the formation of isolated PtCe bimetallic sites that serve as new surface active sites of CO oxidation [26]. Such PtCe sites were also partially re-oxidized to Pt-O-Ce sites under reaction conditions, with low-coordinated oxygen seemingly facilitating an enhanced catalytic activity. These data [26,27] are in line with the finding of Fu et al. that oxidized noble metal species can be more active than the completely reduced ones [28]. Following this study, Wang et al. activated a Pt/CeO_2 catalyst containing Pt-SA sites using H_2 and the CO + O_2 reaction medium, resulting in the formation of PtO_x clusters on CeO_2 [29]. It was concluded that although Pt-O-Ce sites in the Pt-SA/CeO_2 catalyst mediate the oxidation of CO via the Mars-van Krevelen (MvK) mechanism, the oxidation is more efficient on the oxidized PtO_x/CeO_2 catalyst, where Pt-O-Pt sites are involved.

The low-temperature activity can also be triggered by increasing the concentration of Pt on the CeO_2 surface. For example, activation of Pt/CeO_2 samples synthesized by laser ablation in liquid resulted in a catalyst with high CO oxidation activity at room temperature and below −10 °C [9]. Pt loading increase to $\geq$ 8 wt% sharply improved the low-temperature CO oxidation activity of Pt/CeO_2 catalysts [30]. As in some of the afore-mentioned studies, the high activity at very low temperature was tentatively attributed to the emergence of PtO_x clusters, which enable the catalytic CO oxidation on Pt-O-Pt sites. In addition, although the appearance of mobile and reactive oxygen due to the interplay between Pt^{2+} and Pt^{4+} ions in bulk-like positions of ceria made the MvK mechanism operative already at room temperature, the high CO conversion observed *below* 0 °C did not involve such lattice oxygen atoms [30].

In summary, different studies generally agree that reductive pre-treatments in H_2 lead to more active Pt/CeO_2 catalysts for the low-temperature oxidation of CO. There are, however, contradicting views on which state of Pt mediates such high activity: either reduced Pt particles resulting from the pre-treatments or oxidized states of such particles emerging under CO oxidation reaction conditions. Notably, the effects of the combined pre-treatment in H_2 of Pt/CeO_2 catalysts and their exposure to the reaction media on the CO oxidative activity depending on the Pt content are scarcely studied in the literature.

To advance the debate outlined above, we systematically study effects of the reductive and oxidative treatments of Pt/CeO_2 catalysts on their state and activity. We monitor the oxidation state and nuclearity of the Pt species after reduction in H_2, and their oxidation upon exposure to the reaction medium of CO oxidation. Combining catalytic, spectroscopic and microscopy experimental methods with density-functional theory (DFT) calculations, we characterize the transformation of reduced Pt species into PtO_x clusters and analyze the implications for a very high activity of these catalysts below room temperature. We thus identify the conditions at which the oxidation to PtO_x clusters occurs and quantify strong differences in the redox behavior of the catalysts with high and low Pt loadings.

2. Experimental

2.1. Sample preparation

Pt/CeO_2 catalysts were synthesized by co-precipitation as detailed elsewhere [30,31]. A series of catalysts containing 1.1, 7.5 and 14.6 wt% of Pt and calcined at 600 °C were studied after a pre-treatment in either 20%O_2/He at 450 °C (oxidation) or 40% H_2/He at 300 °C (reduction). The corresponding oxidized and reduced samples are nominally designated as 1Pt/CeO_2-Ox, 8Pt/CeO_2-Ox, 15Pt/CeO_2-Ox and 1Pt/CeO_2-Red, 8Pt/CeO_2-Red, 15Pt/CeO_2-Red. The choice of temperature during the pretreatments is motivated as follows. The as-prepared catalysts (after calcination at 600 °C and subsequent contact with air at room temperature) contain adsorbed water that deactivates the samples [30]. Heating the catalyst samples at 450 °C under 20% O_2 in helium removes adsorbed water without altering the oxidation states and particle size of Pt or PtO_x species. This oxidative pretreatment has a similar effect to exposure to reaction conditions at 450 °C, which also removes water and activates the catalyst. For the reductive pre-treatment, we chose a temperature of 300 °C because it recovers reduced forms of the Pt species without noticeable sintering. Exposure at higher temperatures was found to be detrimental to the CO oxidation activity [32].

2.2. Methods

Transmission electron microscopy. The morphology and microstructure of particles were studied by transmission electron microscopy (TEM) using aberration-corrected electron microscopes JEOL JEM-2200FS (at "VTAN" resource center, Novosibirsk State University) and Thermo Fisher Scientific Themis Z (at Boreskov Institute of Catalysis). Both microscopes operated at an accelerating voltage of 200 kV, with the spatial resolution 1.0 Å and 0.7 Å, respectively. Images with a high atomic number contrast were acquired using a high angle annular dark field (HAADF) detector in the scanning-TEM (STEM) mode. The samples for the TEM study were dispersed ultrasonically and deposited on a holey carbon film mounted on a copper grid.

X-ray photoelectron spectroscopy. To characterize the initial (as-prepared) samples, X-ray photoelectron spectra (XPS) were recorded on a KRATOS ES-300 electron spectrometer using MgKα radiation (hν = 1253.6 eV) with 70 W. No sample reduction was observed during the spectra acquisition. The Ce3d line at 916.7 eV was used as a reference for spectra calibration [33]. To

determine the level of surface contamination, high-sensitivity survey spectra were recorded. The chemical composition was calculated from XPS data taking into account atomic sensitivity factors [34]. The original *XPSCalc* software was employed for the deconvolution of experimental spectra into individual components [35–37]. The spectral background of the Pt4f line was subtracted by the Shirley method, and an approximation of the Pt4f and Ce3d doublets was made using Lorentzian and Gaussian functions. *In situ* XPS measurements were performed using the laboratory near-ambient pressure X-ray photoelectron spectroscopy (NAP-XPS) system (SPECS Surface Nano Analysis GmbH, Germany). A special "chamber-in-chamber" design consisted of a NAP cell that allowed studies at pressures from 10^{-9} to 20 mbar, and temperatures from 200 to 773 K (for a detailed description of the setup see [38,39]). NAP-XPS experiments were performed using monochromatic AlKα X-ray radiation. Powder catalysts were pressed into stainless steel wire meshes attached to the sample holder by spot welding. The samples were heated conductively during measurement by electron bombardment of the rear (vacuum) side of the NAP cell, to which the sample holder was attached. The temperature was monitored by a K-type thermocouple welded near the mesh and the pressed sample. The quadrupole mass spectrometer was connected to the first pumping stage to measure the reaction products.

Catalytic activity measurements. The synthesized CO oxidation catalysts were tested in a flow reactor using the temperature-programmed reaction (TPR-CO + O_2) method. The volume of the catalyst samples in the reaction was 0.6 cm^3, and the grains sizes were 0.14–0.25 mm. The samples were heated at a rate 10 °C/min from –10 or –40 °C to 450 °C. These two starting temperatures were chosen depending on the cryostats employed. The reaction mixture of 0.6% vol. CO, 1.0% vol. O_2, 0.5% vol. Ne in flowing He was fed at a rate of 500 cm^3/min, i.e. the gas hourly space velocity (GHSV) of 50 000 h^{-1}. Neon was added as the inert reference for precise calculation of the component concentrations in the reaction mixtures. The concentrations of CO (M/Q = 12, 28), CO_2 (M/Q = 12, 28, 44), O_2 (M/Q = 32), H_2 (M/Q = 2) and H_2O (M/Q = 18) were measured with a quadrupole mass spectrometer RGA 200 (SRS). The partial pressure of each determined M/Q of ions was normalized to the partial pressure of Ne (M/Q = 20). The concentrations of CO, CO_2 and O_2 were monitored using a mass spectrometer at a frequency of 0.35 Hz. When studying the initial stage of reaction ignition, the admission of the reaction medium was accompanied by measurements of CO, O_2 and CO_2 partial pressures and recording the catalyst temperature using a thermocouple mounted directly in the catalyst bed. The experimental conditions similar to those employed in [8,32] (GHSV = 50000 h^{-1}; CO = 0.6 vol% and O_2 = 1.0 vol%) ensure reliable comparison of the present and literature data. From the catalytic data obtained at CO conversion below 100%, the reaction rate was estimated using the formula $W\left(\frac{mmolCO}{molPt\times s}\right)=\frac{C^o_{CO}\times X\times V_{RM}}{\nu}$, where C^o_{CO} is the initial concentration of CO (mmol/cm^3), X is the CO conversion, V_{RM} is the reaction mixture rate (cm^3/sec), ν is the molar content of platinum (mol). The TOF was calculated as $\frac{C^o_{CO}\times X\times V_{RM}}{\nu * Y}$, where Y is the fraction of active Pt determined from XPS.

For the steady-state experiments the 8Pt/CeO_2 catalyst was diluted to eliminate the heat and mass transfer limitations. The diluted catalyst 8Pt/CeO_2† was prepared by grinding, pressing and sieving the mixture of 0.2 g of the 8Pt/CeO_2 catalyst and of 0.3 g of CeO_2 powder. The 8Pt/CeO_2† catalyst contained 0.082 mmol of Pt in 0.25 cm^3 of the 0.14–0.25 mm fraction. The speed of the reaction mixture of 0.6 vol% CO, 1.0 vol% O_2, 0.5 vol% Ne, He-balance was 100 cm^3/min with the CO flow 0.027 mmol CO/min.

X-ray diffraction, Raman spectroscopy, TPR-H_2, analytical and morphological data for the addressed here Pt/CeO_2 catalysts with different Pt contents were reported by us earlier [30,31].

Computational. Spin-polarized DFT calculations were performed using the periodic plane-wave code VASP [40,41]. The generalized-gradient approximation (GGA) type PW91 exchange–correlation functional [42,43] was used. CeO_2 (ceria) can be satisfactorily described using GGA functionals corrected by the on-site Coulombic interaction *U* of Ce 4f electrons. Here, the GGA + *U* scheme [44] with *U* = 4 eV [45–47] (PW91 + 4) was applied. Interactions between core and valence electrons were accounted for via the projector-augmented wave (PAW) method [48]. The Brillouin zone was sampled using only the Γ point. Local positions of atoms were optimized until forces acting on them became smaller than 0.02 eV/Å. The energy difference threshold controlling the convergence of the self-consistent field was set to 10^{-5} eV.

The oxide support was represented by CeO_2(1 1 1) slabs formed of two CeO_2 tri-layers and 4 × 4 surface supercells, with 12 Å of vacuum between the neighboring slabs. Stronger support effects of CeO_2 are expected when more active (1 1 0) or (1 0 0) surfaces of it are considered instead of the most stable (1 1 1) surface modelled here. Positions of Ce and O atoms in the upper CeO_2(1 1 1) tri-layer in contact with the Pt-containing clusters were allowed to relax, while all atoms of the bottom tri-layer remained fixed at the positions defined by the PW91 + 4 optimized ceria bulk lattice parameter 5.40 Å [47]. Positions of atoms in the Pt_6O_n (n = 0 – 12) clusters supported on CeO_2(1 1 1) were obtained by the GOFEE global optimization method [49] as detailed elsewhere [50]. The GOFEE approach uses an algorithm assisted by machine-learning to efficiently explore the configurational space and search for the global minimum (GM) structure. To ensure the quality of the predicted GM, hand-made structures were added to the pool of structures examined by GOFEE. Once the putative GM structures have been calculated for all targeted Pt_6O_n stoichiometries, their Gibbs free energies of formation were evaluated by means of *ab initio* thermodynamics (AITD) [51,52] as specified in [50] at 300 K and oxygen pressure 0.01 atm, mimicking experimental conditions of the present study.

3. Results and discussion

3.1. Catalytic properties of the oxidized and reduced samples

Fig. 1 displays the evolution of CO conversion with temperature for the 1Pt/CeO_2, 8Pt/CeO_2 and 15Pt/CeO_2 catalysts after 2-hour pre-treatments either in 20%O_2/He at 450 °C (oxidative, Ox) or in 40%H_2/He at 300 °C (reductive, Red). After completing the first heating (*up-1*) temperature is decreased (*down*) to the starting point and the second heating cycle (*up-2*) showed how the exposure of the sample to reactants has affected its activity. The second heating was started after reaching a quasi-stationary regime upon exposure to reactants at the starting temperature. T_{10}, T_{50}, T_{90} temperature values at which 10, 50 and 90%, respectively, of CO converted to CO_2 and reaction rates for 1Pt/CeO_2, 8Pt/CeO_2 and 15Pt/CeO_2 catalysts after treatment in O_2 or H_2 during the first and second heating phases in the reaction medium are listed in Table S1.

Fig. 1a shows that the oxidized 1Pt/CeO_2-Ox catalyst is inactive below 100 °C. Heating it to 450 °C in the reaction medium virtually does not change the activity and the temperature dependences of CO conversion after the heating/cooling/heating steps *up-1*, *down*, *up-2* coincide. On the contrary, the reduced 1Pt/CeO_2-Red catalyst is active already below 0 °C with a high room-temperature activity in agreement with literature [8,32]. Fig. 1a and Table S1 demonstrate significantly growing activity of the 1Pt/CeO_2 catalyst after its pre-reduction (1Pt/CeO_2-Red).

At variance with 1Pt/CeO_2-Ox, CO conversion over the catalyst 8Pt/CeO_2-Ox is high already at –40 °C in the first cycle (Fig. 1b),

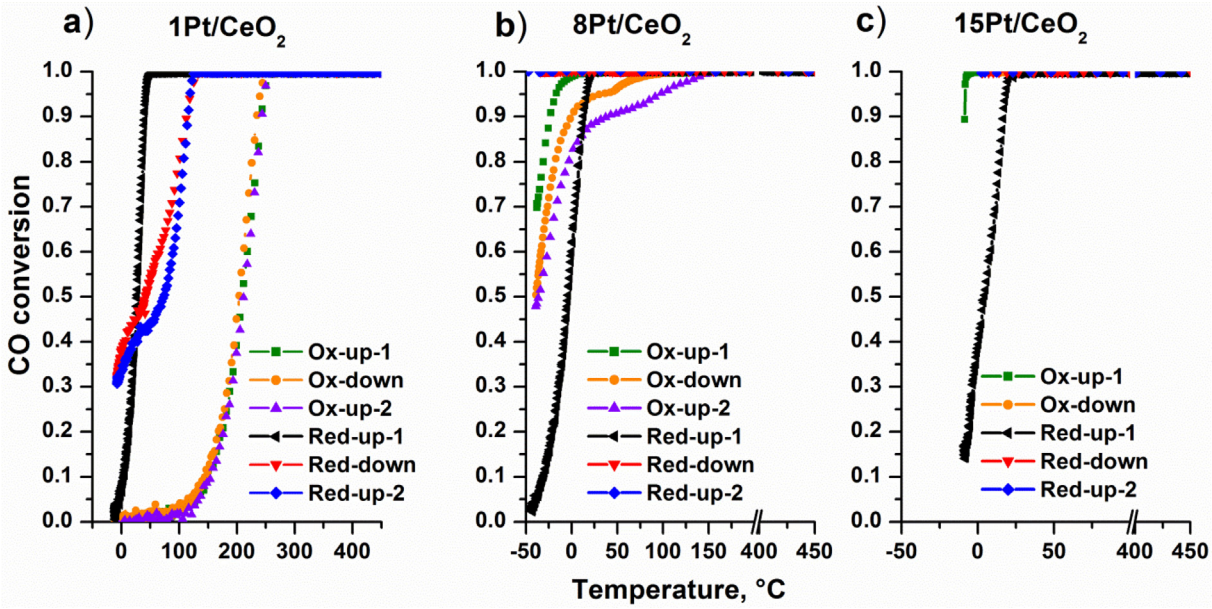

Fig. 1. Temperature dependences of CO conversion for (a) 1Pt/CeO_2, (b) 8Pt/CeO_2 and (c) 15Pt/CeO_2 catalysts after pretreatments in 20%O_2/He at 450 °C for 2 h (Ox) and in 40% H_2/He at 300 °C for 2 h (Red) in the temperature-programmed regime in CO oxidation during the heating *up-1*, the cooling *down* and the second heating *up-2*. (For interpretation of the references to color in this figure legend, the reader is referred to the web version of this article.)

wherein the catalyst 8Pt/CeO_2-Red is much less active (Fig. 1b, Table S1). After the *up-1* heating, CO conversion over 8Pt/CeO_2-Red reaches 100% and remains unchanged over the studied temperature range after the steps *down* and *up-2*. We note that the catalyst ignition (sudden increase of CO conversion) is observed on the reduced catalysts but not on the oxidized ones. The latter are therefore already in their active state at −40 °C and a high conversion is immediately observed when the reaction medium is admitted.

The 15Pt/CeO_2-Ox catalyst (Fig. 1c) shows the initial conversion of virtually 100% at −7 °C, which remains constant upon heating to 450 °C and the next cooling/heating cycles. Initial low-temperature CO conversion of the reduced catalyst 15Pt/CeO_2-Red is lower, but it grows rapidly with temperature elevation. Cooling *down* and heating *up-2* cause complete conversion of CO over the studied entire temperature range, preventing estimates of the reaction rates.

The TPR-CO + O_2 data in Fig. 1 and Table S1 reveal that 1) the catalyst activity sharply increases as the platinum content is raised from 1 to 8%; 2) pre-reduction in H_2 of the low platinum content catalyst (1 wt%) increases the CO oxidation activity at room temperature and below; 3) pre-oxidation of the catalysts with increased platinum contents (8 and 15 wt%) is a more efficient treatment for increasing the catalytic activity than their pre-reduction.

Thus, the pre-reduction of the catalysts is important for directly increasing the activity at 0 °C and lower temperatures, although this does not mean that the reduced states of Pt serve as the active sites at such low temperatures. The CO oxidation activity increase of Pt/CeO_2 catalysts upon reduction agrees with literature [8,18–24,53,54]. The latter studies assign an enhancement of the catalytic activity after reductive treatment in CO or H_2 mainly to the formation of Pt metallic clusters and increased amount of oxygen vacancies. It is commonly accepted that metallic Pt species serve for CO adsorption, whereas O_2 adsorbs on oxygen vacancies and interacts with CO to yield CO_2 [53]. However, the CO oxidation mechanism derived from these published catalytic data is operative only above room temperature. Notably, the reported increased activity of the reduced catalysts was not stationary, not accounting for the heating/cooling cycles and possible re-oxidation of the catalyst by exposure to the reaction mixture [8,32]. This may explain the disagreements between the results of the present work and the literature data on the states of platinum and the sites active in the low-temperature oxidation.

The state of platinum in the catalysts after oxidation and reduction was studied by XPS.

3.2. Oxidation states of the catalysts after the reductive or oxidative treatments

Fig. 2 displays Pt4f and Ce3d spectra of 1Pt/CeO_2 and 15Pt/CeO_2 catalysts after oxidative and reductive treatments.

Pt4f spectrum of the 1Pt/CeO_2-Ox catalyst calcined at 600 °C (Fig. 2a, curve 2) features a single doublet with $E_b(Pt4f_{7/2})$ = 73.1 eV of ions of the single-atom sites [Pt^{2+}-O_4] [15,19,30,55,56]. Pt4f spectrum of the 15Pt/CeO_2-Ox catalyst (Fig. 2a, curve 4) consists of two doublets with $E_b(Pt4f_{7/2})$ = 72.7 and 74.3 eV corresponding to Pt^{2+} and Pt^{4+} ions, respectively [37,57,58]. For the catalysts reduced in H_2, a doublet with $E_b(Pt4f_{7/2})$ = 71.3–71.4 eV (curves 1,3) manifests metallic platinum. These $E_b(Pt4f_{7/2})$ values are slightly higher than for bulk Pt (71.1 eV [34,59]) in line with small positive charge on Pt clusters interacting with ceria [26,60]. According to the data in Fig. 2a the reduction degree of platinum in the 1Pt/CeO_2 catalyst, calculated as the ratio of areas for the metallic and ionic Pt components, is much lower (<20%) than that in the 15Pt/CeO_2 catalyst (>70%). The shift of the Pt4f doublet for Pt^{2+} ions in the 1Pt/CeO_2 sample from 73.1 to 72.7 eV after catalyst reduction reflects association of Pt^{2+}-SA ions into PtO_x clusters, which have characteristically lower $E_b(Pt4f_{7/2})$ [37]. The measured small shift of the Pt4f doublet for Pt^{2+} state to higher $E_b(Pt4f_{7/2})$ in the 15Pt/CeO_2 catalyst after pre-reduction is due to increased relative contributions of Pt^{2+}-SA centers versus PtO_x clusters. In addition, the oxidized catalyst with high Pt content contains Pt^{4+} ions, all reduced by the interactions with H_2. Thus, the redox treatments of the Pt/CeO_2 catalysts enable transitions between the oxidized (curves 2,4) and reduced (curves 1,3) states of platinum.

Ce3d spectra of 1Pt/CeO_2 and 15Pt/CeO_2 catalysts pre-treated in H_2 and O_2 are compared in Fig. 2b. The oxidation and reduction

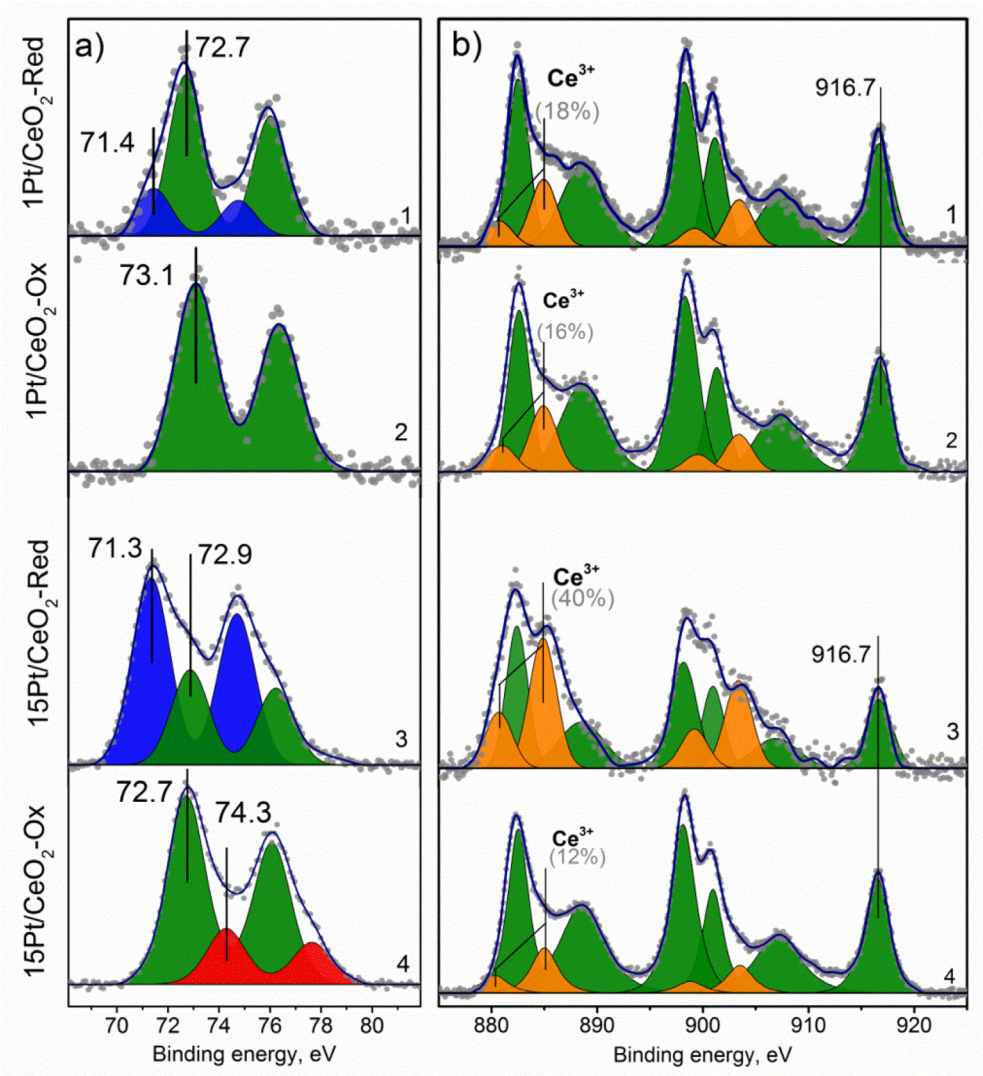

Fig. 2. Pt4f (a) and Ce3d (b) fitted XPS spectra of 1Pt/CeO_2 (curves 1,2) and 15Pt/CeO_2 (curves 3,4) catalysts either after pre-reduction in H_2 at 300 °C (curves 1,3) or after pre-oxidation in O_2 at 450 °C (curves 2,4). The spectra were recorded *ex situ* at room temperature without contact of the catalysts with air. All Pt4f and Ce3d spectra were calibrated against the peak with E_b = 916.7 eV.

degrees of CeO_2 in catalysts can be estimated from Ce3d spectra by the concentration of Ce^{3+} ions with respect to all Ce ions (Ce^{3+} + Ce^{4+}) [33]. Reduction of the 1Pt/CeO_2 catalyst results in a minor increase of the $Ce^{3+}/(Ce^{3+}+Ce^{4+})$ ratio, from 16% (curve 2) to 18% (curve 1). Unlike, the Ce^{3+} concentration notably increased in the reduced 15Pt/CeO_2 catalyst (curve 3), where the $Ce^{3+}/(Ce^{3+}+Ce^{4+})$ ratio 40% should be compared with 12% in the oxidized catalyst (curve 4). The increase of Ce^{3+} concentration after H_2 treatment correlates with the Pt loading indicating active participation of Pt in O vacancy formation in ceria. Pt particles facilitate the migration of O atoms from ceria to supported Pt particles (reverse spillover) [46]. Overall, the Pt4f and Ce3d spectra in Fig. 2 suggest that the studied redox processes involve the participation of $Pt^0/Pt^{\delta+}$, Pt^{2+}, Pt^{4+} and Ce^{3+}, Ce^{4+} centers.

Arrhenius dependences of the CO oxidation reaction rate W (decimal logarithm of W versus 1/T) using the 1Pt/CeO_2-Ox, 1Pt/CeO_2-Red, 8Pt/CeO_2-Ox and 8Pt/CeO_2-Red catalysts obtained by their heating up-1 and up-2 are presented in Fig. 3a.

The relative content of different Pt species derived from XPS and the activity measurements allow quantifying the catalytic activity associated to each state of platinum. Fig. 3b shows the CO oxidation reaction rates normalized to the content of each type of active sites (TOF) at –25 °C and at 0 °C. We have used the 1Pt/CeO_2 catalyst as an example because the three relevant active species (Pt^{2+} single atoms, metallic Pt particles, and oxidized PtO_x particles) could be formed in it by means of different treatments. The oxidative pre-treatment by O_2 generated Pt^{2+} single atoms only. The reduction by H_2 resulted in the transformation of 20% of Pt^{2+}-SA to metallic Pt clusters (fraction Y of Pt used for TOF calculations is 0.2). All such metallic Pt clusters were further re-oxidized by the reaction mixture giving rise to the formation of PtO_x clusters. Since PtO_x and Pt particles are significantly more active than Pt^{2+}-SA at –25 °C and at 0 °C (see below), the contributions of the single-atom species to the turn-over frequencies for the reduced and re-oxidized clusters were neglected.

After the first oxidative treatment, CO conversion at –25 °C and at 0 °C is too low to be measured directly. The reaction rate value for the Pt^{2+}-SA centers was therefore extrapolated from the reaction rates at higher temperatures (Fig. 3a), resulting in TOF = 1×10^{-6} and 4×10^{-6} sec^{-1} at –25 and 0 °C, respectively. After the treatment in H_2, the 1Pt/CeO_2 catalyst contains Pt^0 active sites, which notably increase the reaction rate compared to the Pt^{2+}-SA sites (TOF = 1.1×10^{-3} and 1.19×10^{-2} sec^{-1} at –25 and 0 °C, respectively). After re-oxidation of the Pt^0 species to PtO_x by exposure

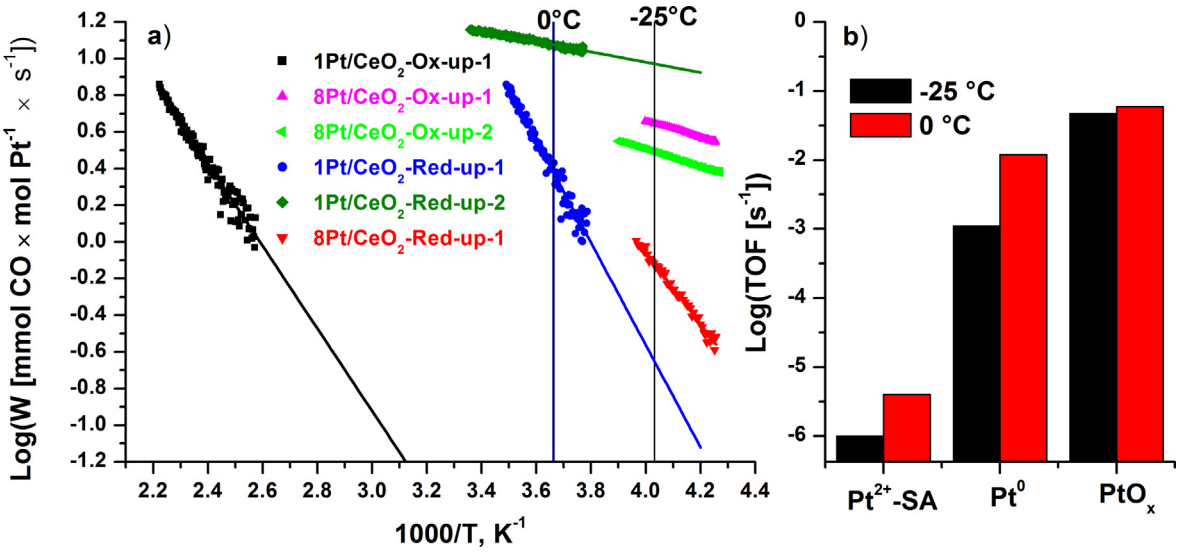

Fig. 3. a) Arrhenius dependences of the CO oxidation reaction rate W (decimal logarithmic W versus 1/T) using the 1Pt/CeO_2-Ox, 1Pt/CeO_2-Red, 8Pt/CeO_2-Ox and 8Pt/CeO_2-Red catalysts obtained by their heating treatments up-1 and up-2. Straight lines for the 1Pt/CeO_2 catalysts indicate extrapolated values; b) Log(TOF) at –25 and 0 °C for the 1Pt/CeO_2 catalysts Ox-up-1, Red-up-1 and Red-up-2 containing Pt^{2+}-SA, Pt^0, and PtO_x active forms after pre-treatments by $O_{2\ (Ox)}$, H_2 (Red), and the CO + O_2 reaction mixture (Ox-up-2, Red-up-2), respectively.

to the reaction mixture at 450 °C, the reaction rate dramatically increases (TOF = 4.72 × 10^{-2} and 5.94 × 10^{-2} sec^{-1} at –25 and 0 °C, respectively).

The strong dependence of the TOF on the Pt species present in different states of the 1Pt/CeO_2 catalyst (Fig. 3b) is related to different activation energies (see Table S1). Pt^{2+}-SA and Pt^0 sites are characterized by activation energies of 10 and 13 kcal/mol, respectively, whereas the calculated activation energy for PtO_x sites is 1.3 kcal/mol. This low value is consistent with the very high activity at sub-ambient temperatures and indicates that the reaction on Pt^{2+}-SA and Pt^0 sites operates through a different mechanism than on PtO_x particles.We note that the activation energy for the 1Pt/CeO_2 catalysts exposing PtO_x particles is identical to the energy previously obtained for oxidized 8Pt/CeO_2 and 20Pt/CeO_2 catalysts [30]. This further indicates that PtO_x clusters provide the main sites for the low-temperature CO oxidation and that the corresponding activity below 0 °C is related to the amount of oxidized PtO_x particles.

Isothermal experiments at –37 °C allow evaluating the activity and stability of the catalyst under steady state conditions and confirming that the formation of CO_2 below 0 °C occurs because of a catalytic reaction and not through the reduction of the catalysts (Fig. S1). We note that the internal and external diffusion limitations and the heat transfer limitation were negligible in this kinetic experiment (see Supplementary Material).

3.3. Interaction of reaction medium with the catalysts

3.3.1. Peculiarities of the catalysts reoxidation during CO oxidation

To elucidate the action of oxidized and reduced states of platinum in the Pt/CeO_2 catalysts for CO oxidation, we examined the temperature genesis of the effect exerted by the reaction medium on the pre-oxidized and pre-reduced states of the catalysts starting from –40 °C. For that, the concentrations of the reactants and product of the CO + O_2 → CO_2 reaction were analyzed depending on time upon admission of the reaction medium to the oxidized and reduced Pt/CeO_2 catalysts. The admission to pure CeO_2 support (without Pt) is shown in Fig. S2. This kinetic experiment for pure CeO_2 reveals a) no formation of CO_2 at low temperature, with its start only after heating above 100 °C; b) virtually inappreciable temperature jump after the admission of the reactants; c) no improvements in the catalytic activity of the pure CeO_2 sample after its pre-reduction in H_2 at 300 °C.

The interaction of CO and O_2 was studied with catalysts oxidized in 20%O_2/He at 450 °C. Panels a, c, e in Fig. S3 show the dependence of CO, CO_2 and O_2 concentrations and temperature on time after admission of CO + O_2 flow to the reactor (0 point on the time axes) for the oxidized 1Pt/CeO_2-Ox, 8Pt/CeO_2-Ox and 15Pt/CeO_2-Ox catalysts. Heating of each catalyst began after achieving (pseudo-)stationary concentrations of reactants and products.

Practically no change of CO, CO_2 and O_2 concentrations upon feeding the reaction mixture to the 1Pt/CeO_2-Ox catalyst at –10 °C and subsequent heating documents absent reaction below 120 °C. The reactants admission to the 8Pt/CeO_2-Ox catalyst caused at –40 °C a decrease of CO and O_2 concentrations along with CO_2 concentration increase revealing CO conversion of ca. 70%. For the 15Pt/CeO_2-Ox catalyst, the concentrations of reactants upon their admission at –10 °C and of CO_2 change similarly as for the catalyst 8Pt/CeO_2-Ox.

The interaction of CO and O_2 was studied for the 8Pt/CeO_2-Red catalyst (pre-reduced in 40%H_2/He at 300 °C). Fig. 4 shows the evolution of CO, CO_2 and O_2 concentrations and temperature after admission of CO + O_2 flow to the reactor (see Fig. S3 for the dependencies for all studied reduced catalysts).

The reactants admission to the reduced catalysts 1Pt/CeO_2-Red, 8Pt/CeO_2-Red and 15Pt/CeO_2-Red causes a pronounced temperature jump (Fig. 4, Fig. S4) mainly due to CO and O_2 adsorption, indicating initial partial oxidation of the catalysts. No formation of CO_2 was observed in the low-temperature range. The reaction is initiated only after starting the reactor heating, as evidenced by a simultaneous decrease of CO and O_2 concentrations and a concomitant growth of CO_2 concentration. Also, there is a deviation of temperature from the linear dependence of the heating rate in the interval 25–50 °C (see Fig. S5). This temperature maximum is accompanied by strong O_2 consumption and CO_2 formation above the stoichiometric value. Both the temperature deviation from the expected values and the abrupt changes in the O_2 and CO_2 concentrations are related to oxygen consumption by Pt species pre-reduced with H_2. The calculated amounts of consumed O_2 and

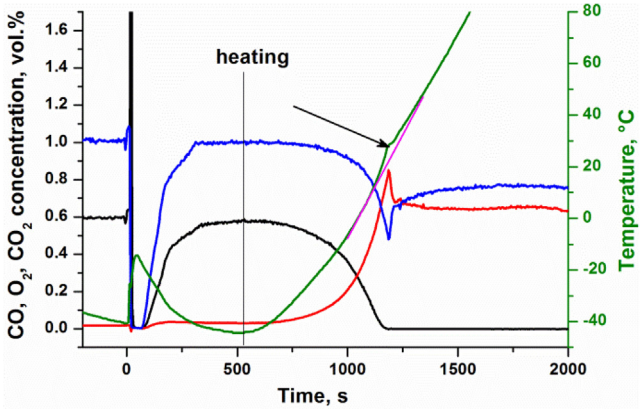

Fig. 4. Evolution with time of CO (black), CO_2 (red) and O_2 (blue) concentrations and temperature upon switching on feeding of the reaction mixture to the reactor (zero on the time axes) for the reduced 8Pt/CeO_2-Red catalyst. Vertical lines designated as "heating" show the onset of catalyst heating started at achieving a quasi-stationary regime after the reactants admission at low temperature. Arrows indicate the temperature maximum due to the catalyst overheating; the expected curve without the overheating is shown in pink. (For interpretation of the references to color in this figure legend, the reader is referred to the web version of this article.)

released CO_2 for 8Pt/CeO_2-Red catalyst are similar, 39 and 42 μmol/g, respectively. For 15Pt/CeO_2-Red catalyst the calculated amounts of consumed O_2, 157 μmol/g, and of CO_2 released during this sharp O_2 consumption, 159 μmol/g, are essentially the same. Thus, the amount of consumed O atoms is twice as large as the amount of released CO_2 molecules, suggesting that for every O atom consumed for the reaction with CO, a second O atom is consumed for the re-oxidation of the Pt species. During this step, the calculated ratios of consumed O_2 to total amount of Pt, O_2/Pt, are ca. 0.1 for 8Pt/CeO_2-Red and 0.2 for 15Pt/CeO_2-Red catalysts. The simultaneously occurring oxidation of CO and partial re-oxidation of the reduced platinum suggest that these processes involve the same intermediate, possibly of the $(O_2\text{-}CO)^*$ type.

Major interactions of the reactants with the pre-reduced catalysts at low temperatures appear to occur in two steps, at –40 °C and in the interval 25–50 °C (Fig. S3). Fig. 5 shows that both the O_2 consumption and the temperature response are more significant during the initial reactants admission at/below –10 °C. Thus, in the initial step the catalyst is intensely re-oxidized with pronounced exothermicity due to forming strong chemical bonds. Because the pre-reduced catalysts have higher concentrations of Ce^{3+} and O vacancies than the oxidized ones (see Fig. 2), interaction of Pt/CeO_2-Red with oxygen initially results in the formation of Ce-O-Ce and Ce-O-Pt bonds upon healing O vacancies. Then, heating of the catalyst in the reaction mixture at 25–50 °C leads to further oxidation of (metallic) platinum, with the formation of Pt-O-Pt bonds. Results of these two steps are hereafter referred to as the first and second oxidation stages.

From the data in Fig. 5, we can estimate the amounts of O used for healing vacancies or for oxidizing metallic Pt. We assume that at −40 °C most O is used for healing vacancies. The fractions of vacancies healed at −40 °C would therefore be 24, 37 and 67% for 1Pt/CeO_2, 8Pt/CeO_2, 15Pt/CeO_2, respectively. Note that this corresponds to molar O/Pt ratios of 12.4, 2.8, and 2.6, respectively. Thus, the O content increased from 1Pt/CeO_x to 1Pt/$CeO_{x+0.12}$, from 8Pt/CeO_y to 8Pt/$CeO_{y+0.18}$, and from 15Pt/CeO_z to 15Pt/$CeO_{z+0.33}$. The oxygen uptake at ∼ 30 °C was, in turn, assumed to oxidize mostly Pt, and the calculated molar ratios of consumed O_2 to total amount of Pt, are ca. 0, 0.1, and 0.2 for the 1Pt/CeO_2, 8Pt/CeO_2-Red, and 15Pt/CeO_2-Red catalysts, respectively.

3.3.2. Partial and complete reoxidation of pre-reduced catalysts

Besides the two re-oxidation stages underwent by the reduced catalysts at –40 °C and in the interval 25–50 °C (Fig. 5) these catalysts undergo further transformations upon heating to higher temperatures. The fraction of re-oxidized platinum beyond the second re-oxidation stage at 25–50 °C and the effect on catalytic activity were estimated from TPR-CO-O_2 experiments performed with freshly prepared 8Pt/CeO_2-Red samples in a similar way as the experiment whose results are shown in Figs. 1 and 4. This time, however, one 8Pt/CeO_2-Red sample was heated to ∼ 60 °C, with subsequent cooling to –40 °C and heating to ∼ 60 °C. Another freshly prepared 8Pt/CeO_2-Red sample was heated to 450 °C, cooled to –30 °C and again heated to 450 °C. The obtained temperature dependencies of CO and O_2 conversions are shown in Fig. 6.

The CO conversion dependence for the catalyst reduced in hydrogen (Fig. 6) is consistent with the data in Fig. 1 obtained during the first heating of the catalyst to 60 °C. Cooling and subsequent heating led to a slight decrease in CO conversion and the anomalously high activity at very low temperatures was no longer observed. The similar dependences of CO, CO_2 and O_2 concentrations in this experiment (see Fig. S6) with the data in Fig. 4 indicate that at temperature below 50 °C, the catalyst heating and cooling in the reaction mixture are accompanied by the partial, rather than complete, oxidation of platinum.

Fig. 6b displays the dependences of CO conversion for the heating/cooling cycle in the –30 to 450 °C range. The concentration and temperature dependences obtained upon heating are shown in Fig. S7. These data match the data in Fig. 1 illustrating again that heating to 450 °C transforms the catalysts to exhibit exceptionally high activity below 0 °C. Namely, the complete conversion of CO is observed at –30 °C upon cooling and repeated heating of the catalyst.

Relating the transformations of the catalyst to its O_2 uptake, Fig. 6 c, d show the oxygen conversion during the first heating of the 8Pt/CeO_2-Red catalyst to 60 and 450 °C. The clearly over-stoichiometric oxygen conversion in the temperature range 10–60 °C manifests the second re-oxidation stage of the pre-reduced catalyst. Upon heating to 450 °C, another over-stoichiometric O_2 conversion takes place at 145–345 °C with a maximum at 265 °C. Here, the molar ratio between consumed O_2 and Pt is 0.34. This is the third and final re-oxidation step, upon which all reduced platinum becomes oxidized.

According to XPS data (Fig. 6 e, f), the second re-oxidation stage at 10–60 °C does not cause complete platinum oxidation. The first observed state $E_b(Pt4f_{7/2})$ = 71.7 eV can be attributed to $Pt^{\delta+}$ – atoms of metallic platinum contacting with oxygen of the oxide support or oxidized platinum. The second state $E_b(Pt4f_{7/2})$ = 73.0 eV is often assigned to single-atom platinum species (Pt-SA) in a Pt^{2+}-like state. Because clusters of reduced platinum can be oxidized, these species may correspond to Pt^{2+} ions located along the cluster perimeter, for which the oxygen environment is similar to that of single platinum ions in the O_4 pockets on the CeO_2 surface.

Heating of the reduced sample to 450 °C leads to the complete re-oxidation of platinum. The main species with E_b = 72.8 eV corresponds to Pt^{2+} ions in PtO_x clusters. The second species characterized by E_b = 74.8 eV and lower intensity corresponds to Pt^{4+}. Importantly, these states of platinum are the same as the states present in the as-prepared catalyst after its calcination.

3.3.3. Pt states after re-oxidation of reduced catalysts: XPS and HRTEM studies

To establish how the uptake of O_2 affects oxidation states of Pt, differently treated 8Pt/CeO_2 catalysts were studied by XPS and high-resolution transmission electron microscopy (HRTEM) (see Figs. 7-8). In particular, we compared the 8Pt/CeO_2 catalyst i) as-prepared (calcined at 600 °C), ii) after two heating/cooling runs

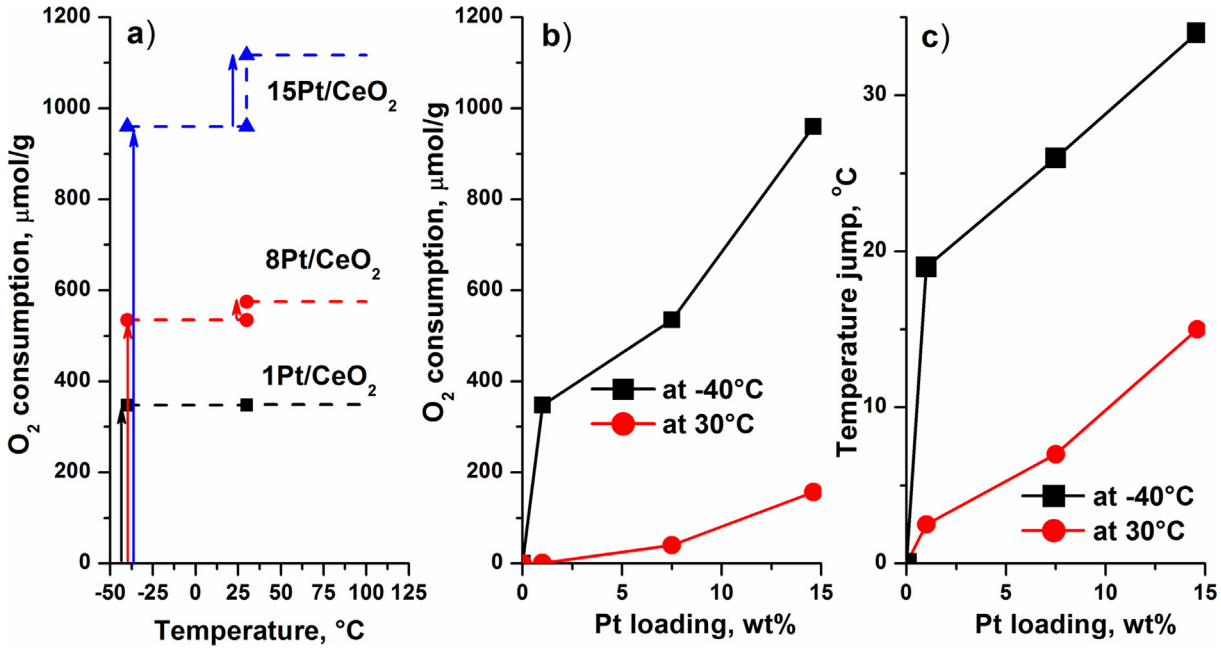

Fig. 5. a) Temperature dependence of the o_2 amount consumed for oxidizing the catalysts 1Pt/CeO_2-Red, 8Pt/CeO_2-Red and 15Pt/CeO_2-Red upon admission of the reaction mixture; b) Dependences of the O_2 consumption at –40 °C and in the interval 25–50 °C on Pt loading in the catalysts; c) Temperature jump (response) of the reduced catalysts upon CO + O_2 admission followed by heating of the reactor. These data were calculated from the time dependencies of the O_2 consumption and of the CO_2 evolution shown in Fig. S3. (For interpretation of the references to color in this figure legend, the reader is referred to the web version of this article.)

of CO + O_2 reaction to 450 °C (see also Figs. 1, 2, and 6), and iii) after reduction in 40%H_2/He at 300 °C and re-oxidation in 20%O_2/He at room temperature (the treatment is hereafter designated as Red-Ox-RT). The latter state represents the state of the catalyst formed after the first two re-oxidation stages (occurring at –40 °C and at 30 °C).

The Pt4f spectrum of the as-prepared catalyst contains two doublets with $E_b(Pt4f_{7/2})$ = 73.0 and 74.6 eV, which correspond to Pt^{2+} and Pt^{4+} ions in the ceria lattice (Fig. 7, curve 1) [30,56]. The catalyst state after TPR-CO + O_2 cycles up to 450 °C does not change significantly (Fig. 7, curve 2), with only slight abundance increase of the Pt^{2+} species relative to Pt^{4+} ones. However, the Red-Ox-RT treatment changes the composition of surface platinum species both quantitatively and qualitatively (Fig. 7, curve 3), exhibiting three states of platinum characterized by $E_b(Pt4f_{7/2})$ = 71.4, 72.7, and 74.1 eV. The last two peaks can be attributed, similar to the as-prepared catalyst, to Pt^{2+} and Pt^{4+} ions, respectively. These peaks are slightly shifted towards lower $E_b(Pt4f_{7/2})$ values with respect to those of the Pt^{2+} and Pt^{4+} species in the as-prepared catalyst. The binding energy decrease by 0.3 eV for the Pt^{2+} species may be caused by the assembly of Pt^{2+} ions (grouping of [Pt^{2+}-O_4] fragments). The decrease of $E_b(Pt4f_{7/2})$ for Pt^{4+}may be related to lowering the coordination of Pt^{4+} cations by O atoms, likely due to creating nearby O vacancies [30].

Finally, $E_b(Pt4f_{7/2})$ = 71.4 eV of the third state of platinum is slightly higher than $E_b(Pt4f_{7/2})$ = 71.1 eV of the metallic state in the bulk phase with 12-coordinated Pt atoms [34,59]. Such slightly shifted $E_b(Pt4f_{7/2})$ peak has been assigned to $Pt^{\delta+}$ atoms of Pt clusters with a small positive charge due to interactions with O atoms of ceria [60–63]. Note that particle size effects alone would lead instead to $E_b(Pt4f_{7/2})$ shifts in the opposite direction with the peaks at 70–71 eV depending on the coordination of atoms and the size and shape of clusters [64].

Thus, the Pt4f spectra reveal that due to the re-oxidation of reduced platinum between –40 °C and 25–30 °C, a half of Pt atoms becomes ionic in three different states $Pt^{\delta+}$, Pt^{2+} and Pt^{4+}.

Ce3d spectra of the 8Pt/CeO_2 catalyst recorded after its calcination or exposure to the reaction mixture estimate the Ce^{3+}/(Ce^{3+}+-Ce^{4+}) ratio as 15–16% (Fig. S8). The ratio remains basically unchanged after the Red-Ox-RT treatment indicating that the oxidation of Ce^{3+} ions occurs below room temperature.

The nature of highly dispersed forms of platinum in the Pt/CeO_2 catalysts was studied using high-resolution TEM and HAADF-STEM. Isolated Pt atoms in the 1Pt/CeO_2 catalyst were observed on HAADF-STEM images as bright dots with a higher contrast against the background of ceria (Fig. 8a). The initial catalyst contains Pt only as single atoms; no evidence of Pt particles was obtained. The Red-Ox-RT treatment led to spatial redistribution and coalescence of Pt atoms in the catalyst (Fig. 8b). In addition to single Pt atoms, the HAADF-STEM monitored one- and two-dimensional species consisting of several Pt atoms. Larger Pt species with the size of 0.3–0.8 nm were also observed, which can be considered as quasi-two-dimensional Pt rafts and three-dimensional few-layer Pt clusters. Notably, platinum clusters were predominantly located on defects of ceria support, such as steps and inter-crystalline boundaries.

The Red-Ox-RT treatment similarly affects the state of platinum in catalysts with a high Pt content of 8% or more. Multiple Pt clusters can be easily detected using conventional HRTEM method, but they are absent in the HRTEM images of the initial catalysts (Fig. 8 c-d, Fig. S9).

The introduction of 8 – 15 wt% Pt in Pt/CeO_2 catalysts negatively affects the stability of atomically dispersed forms of platinum under the action of the electron beam, which makes it difficult to study them in HAADF-STEM mode. Under normal imaging conditions, the Pt atoms migrate rapidly agglomerating in sub-nano clusters [30]. To examine the initial atomically-dispersed state, the beam current was noticeably reduced and the studied samples areas were those not illuminated by electron beam before. At the beam current held below 10 pA, the 8Pt/CeO_2 catalyst was rather stable during several consecutive scans, only a slight movement of Pt atoms occurred (Fig. S10). In the HAADF-STEM image

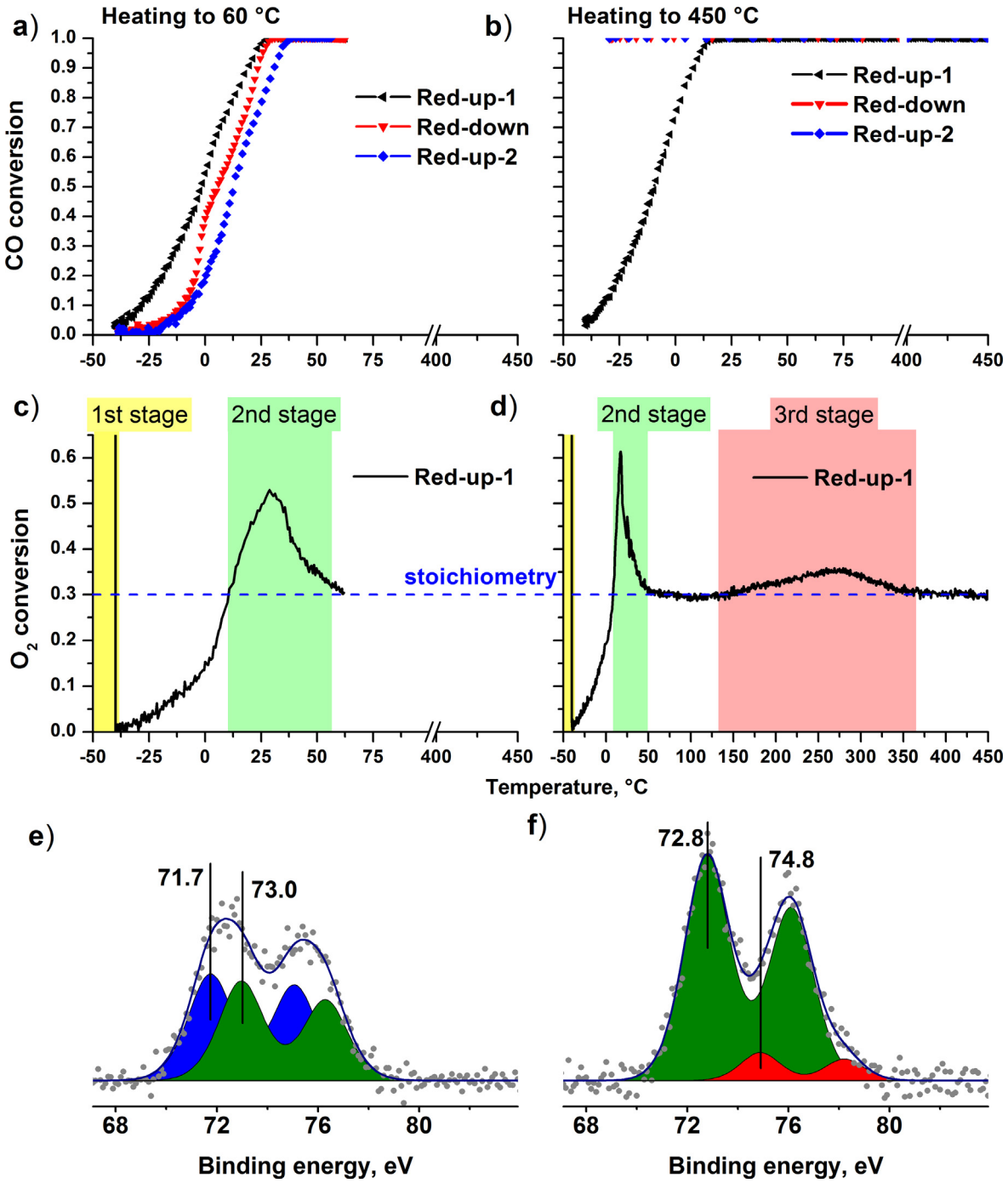

Fig. 6. Temperature dependences of CO conversion (a, b) and O_2 conversion (c, d) for the 8Pt/CeO_2-Red catalyst during TPR-CO-O_2 upon heating to 60 °C (a, c) and 450 °C (b, d); curve-fitted Pt4f XPS spectra of the 8Pt/CeO_2-Red sample after heating to 60 °C (e) and 450 °C (f), see color coding in Fig. 2a. (For interpretation of the references to color in this figure legend, the reader is referred to the web version of this article.)

obtained by the first scan with low beam current (Fig. 8e) there are numerous bright dots standing out against the ceria background which evidence the presence of Pt single atoms (see yellow circles). In some areas of the sample one can also see small species consisting of several agglomerated Pt atoms on the ceria surface (marked with red circles). Unfortunately, it cannot be determined whether such clusters were present initially in the catalyst, or formed under the action of the electron beam (despite the low current used). Increased beam current led to the rearrangement of Pt atoms with agglomeration on ceria surface into 2D raft-like structures and 3D-sub-nano clusters located on the defects of the support, especially at the inter-crystalline boundaries (Fig. S10). Such *in-situ* observation of changes in the location of Pt atoms and structures enables investigation of the processes which can occur under the reductive action of the reaction medium. The size of the Pt clusters formed in 8Pt/CeO_2 and 15Pt/CeO_2 after Red-Ox-RT treatment does not exceed 1.5 nm, and therefore large Pt-containing structures are not formed in the catalysts. This indicates the strong metal-support interaction in the studied system, which stabilizes platinum in a highly dispersed state. However, we rule out that the metal-support interaction results in a partial encapsulation of Pt particles by ceria upon the reductive pretreatment. Such encapsu-

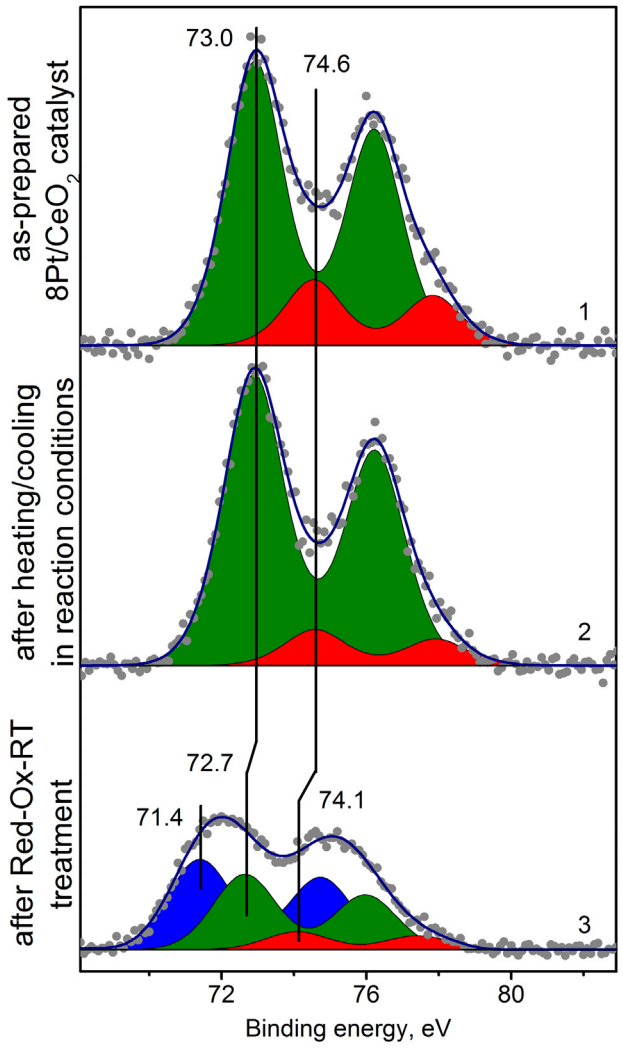

Fig. 7. Fitted Pt4f spectra of the 8Pt/CeO_2 catalyst: (1) as-prepared; (2) after two heating/cooling runs of CO + O_2 reaction to 450 °C (see also Figs. 1, 2, and 6); (3) after Red-Ox-RT treatment. Integrated $Pt^0/Pt^{\delta+}$, Pt^{2+} and Pt^{4+} peaks are colored in blue, green and red, respectively. (For interpretation of the references to color in this figure legend, the reader is referred to the web version of this article.)

lation can occur above 530 °C [65], significantly higher than temperatures employed in the present study; accordingly, the TEM images do not reveal formation of ceria overlayers on Pt particles.

3.3.4. Steps of re-oxidation of metallic platinum species during CO + O_2 reaction

The re-oxidation of 1Pt/CeO_2-Red, 8Pt/CeO_2-Red and 15Pt/CeO_2-Red catalysts depends on the contents of different states of platinum. Fig. 9 illustrates the re-oxidation of Pt starting with metallic species analyzed using XPS in Fig. 2. The 1Pt/CeO_2-Red catalyst contains 20% of metallic Pt (primarily as very small $[Pt_n]^0$ clusters and single Pt^0 atoms) and 80% of Pt as Pt^{2+}-SA centers (Fig. 2). This catalyst is re-oxidized essentially in a single step (Fig. 9a), mainly forming more Pt^{2+}-SA sites relevant for the catalytic activity only above 100 °C. A minor fraction of $[Pt_n]^0$ clusters is likely transformed into partially oxidized clusters. CO oxidation at low temperatures is related to the presence of thus formed PtO_x sites. However, concentration of the latter in the catalyst with so low Pt loading is insufficient for a noticeable low-temperature CO conversion.

Re-oxidation of the high Pt-loaded catalysts is more complex. Unlike the 1Pt/CeO_2-Red catalyst the 15Pt/CeO_2-Red catalyst contains > 70% of metallic Pt and < 30% of Pt as Pt^{2+}-SA centers (Fig. 2). The re-oxidation of the high Pt-loaded catalysts at –40 °C begins with filling O vacancies occurring when the metallic clusters are covered by CO. The latter $CO_{ads}/[Pt_n]^0$ state (second image in Fig. 9b) inhibits CO oxidation by self-poisoning below 30 °C. Above this temperature competitive adsorption of oxygen and CO enables CO oxidation accompanied by partial oxidation of $[Pt_n]^0$ clusters with the formation of Pt-O-Pt bonds (third image in Fig. 9b).

The suggested partial oxidation of Pt particles is in line with the formation of PtO_x species with Pt-O-Pt sites reported by Wang et al. [29]. It is also consistent with the results of the present work showing the consumption of an amount of O_2 able to oxidize 10% and 20% of metallic platinum in the 8Pt/CeO_2-Red and 15Pt/CeO_2-Red catalysts, respectively.

The second oxidation of the Pt content in the 8Pt/CeO_2-Red and 15Pt/CeO_2-Red catalysts takes place at a temperature of ca. 30 °C in the presence of the reaction mixture. An intense O_2 consumption is observed at these conditions, accompanied by the formation of CO_2, sharp elevation of temperature and growth of CO conversion to 100%. Our experiments reveal that ca. one half of the gas-phase O_2 is consumed for the formation of CO_2, while the other half of O_2 is consumed for the oxidation of reduced Pt species.

The experimental data on the second oxidation of metallic platinum clusters by the reaction mixture CO + O_2 can be interpreted as proposed by Iglesia and co-workers and by Beniya and Higashi [66,67]. In particular, the O_2 activation step can include the participation of CO via the formation of an OO-CO* intermediate. The latter decomposes to CO_2 and releases atomic oxygen that oxidizes platinum to PtO_x. Such CO-assisted O_2 dissociation pathway lowers the activation barrier compared to the unassisted O_2 dissociation on Pt nanoparticles [66,67].

The present work shows that despite the active oxygen consumption at 30 °C the reaction mixture does not completely re-oxidize platinum clusters of the reduced high-loading catalysts at temperatures from –40 to 30 °C. The complete oxidation by the reaction medium with the formation of PtO_x clusters essentially without Pt-Pt bonds requires notably higher temperature and finishes at ca. 350 °C, as shown in Fig. 6d. This point corresponds to the formation of Pt_nO_m clusters, in which the m:n ratio reaches a maximum below 2.

The present study suggests that the action of H_2 is related to the transformation of single Pt^{2+} atoms and similar cationic species into clusters of metallic platinum $[Pt_n]^0$, whose subsequent re-oxidation produces Pt_nO_m clusters featuring very different adsorption and reaction properties. Thus, in line with [19–22], H_2 does not only reduce platinum ions, but also induces their aggregation into metallic clusters serving as precursors for the catalytically active Pt_nO_m clusters formed upon admission of CO oxidation reactants.

3.4. In situ near-ambient pressure XPS study of CO + O_2 reaction

NAP-XPS can directly trace the evolution of Pt species under conditions mimicking the experimental reaction conditions. For that the 15Pt/CeO_2 catalyst exposed to the CO + O_2 reaction gas mixture was studied by NAP-XPS. The initial 15Pt/CeO_2 catalyst was pre-treated in oxygen at 450 °C (Fig. S11a, curve 1), revealing after that only the oxidized Pt species – Pt^{2+} and Pt^{4+} ions characterized by $E_b(Pt4f_{7/2})$ = 72.6 and 74.1 eV, respectively.

Thus, the NAP-XPS data corroborate that under the steady-state CO oxidation conditions, active states of platinum are Pt^{2+} and Pt^{4+} cations in the form of single atoms and PtO_x clusters in line with TEM data (Fig. 8). The composition of the platinum species is adjusted under the action of the reaction medium and temperature. Importantly, no state of metallic Pt was observed in the entire scrutinized temperature range, when the ignition and development of the reaction occurred. These data strongly suggest that

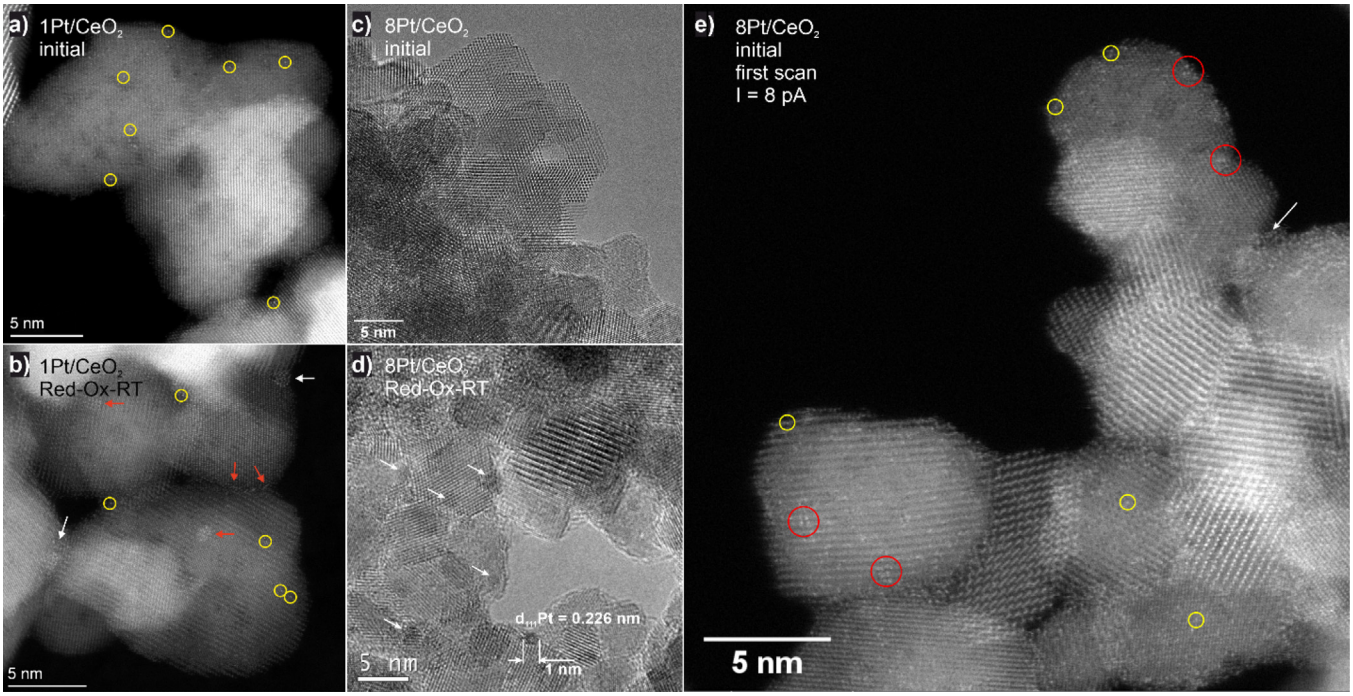

Fig. 8. a) HAADF-STEM image of the initial $1Pt/CeO_2$ catalyst; b) HAADF-STEM image of the $1Pt/CeO_2$ catalyst after Red-Ox-RT treatment; c) HRTEM image of initial $8Pt/CeO_2$ with no evidence for Pt clusters; d) HRTEM image of $8Pt/CeO_2$ catalyst after Red-Ox-RT treatment showing numerous Pt clusters; e) HAADF-STEM image of the initial $8Pt/CeO_2$ catalyst: first scan with a low beam current, where most of platinum is present in atomically-dispersed state. Yellow circles – single Pt atoms, red circles – several agglomerated Pt atoms, red arrows – flat Pt species consisting of several Pt atoms, white arrows – Pt clusters. (For interpretation of the references to color in this figure legend, the reader is referred to the web version of this article.)

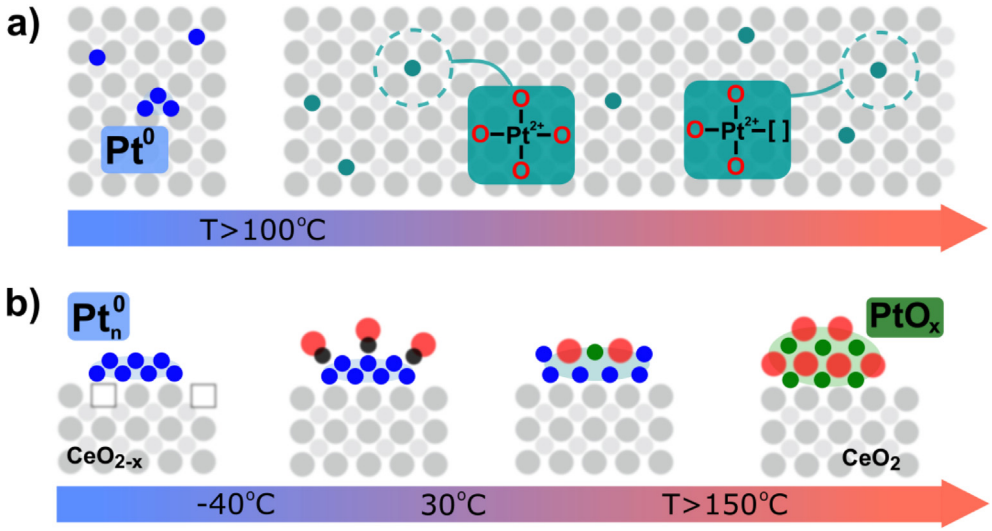

Fig. 9. Schematic re-oxidation of different platinum metallic species on ceria during CO + O_2 reaction as a function of temperature: a) Pt^{2+}-SA and $[Pt_n]^0$ clusters, very small n values; b) $[Pt_n]^0$ clusters, larger n. Color coding: metallic Pt atoms – blue; Pt cations Pt^{2+}-SA in the pristine or O-defective square-planar coordination by lattice O anions – turquoise; cationic Pt atoms in PtO_x clusters – green; ceria support – grey. Left panel in b) shows the initial $[Pt_n]^0$ cluster anchored to reduced ceria. At T > 30 °C CO_{ads} layers covering Pt_n clusters transform into O_{ads} layers accompanied by partial oxidation of the clusters. At T > 150 °C the Pt clusters start to transform into fully oxidized Pt_nO_m structures with the oxidation process completed around 350 °C. (For interpretation of the references to color in this figure legend, the reader is referred to the web version of this article.)

the key active sites for the ignition and achieving maximum conversion of CO oxidation are provided by oxide PtO_x clusters.

3.5. Ceria-supported PtO_x clusters and CO adsorption on them: Results of DFT calculations

Despite indications that Pt particles can be oxidized under various conditions [16,25,29–31,46], their geometry, stability, electronic structure and reactivity are still unclear. Thus, we globally optimized the structure of supported on CeO_2 PtO_x clusters with varying stoichiometry and compared their stability with respect to the corresponding metallic Pt clusters and atomically dispersed Pt^{2+}-SA species.

The global optimization of the structure of Pt_6O_m (m = 0 – 12) clusters supported on CeO_2 was performed using the GOFEE code as outlined in Section 2.2. Formation energies of the obtained glo-

bal minimum (GM) structures are shown in Fig. 10. We present these data using different references to illustrate the relative stability of the three relevant types of species.

Fig. 10a displays the reaction energies of the Pt_6 cluster supported on $CeO_2(1\,1\,1)$ with gas-phase O_2 ($Pt_6/CeO_2 + m(½O_2) \rightarrow Pt_6O_m/CeO_2$) at 0 K (DFT energies, blue bars) as well as at 300 K and p_{O_2} = 0.01 atm (Gibbs free energies, orange bars). This clearly shows that small Pt clusters anchored on ceria are thermodynamically unstable and undergo oxidation already at very low O_2 pressures. We note that Pt clusters can dissociate O_2 molecules with essentially vanishing activation barriers, partly due to the flexibility of Pt atoms [70]. Therefore, adsorbed O_2 readily dissociates into O atoms, oxidizing the Pt clusters. The stability trends revealed by both DFT energies and Gibbs free energies of the oxidative reactions are similar and indicate that Pt_6/CeO_2 clusters are considerably stabilized by interactions with oxygen until reaching the Pt_6O_9 stoichiometry. After that, the addition of O atoms becomes unstable with respect to O_2 in the gas phase reservoir.

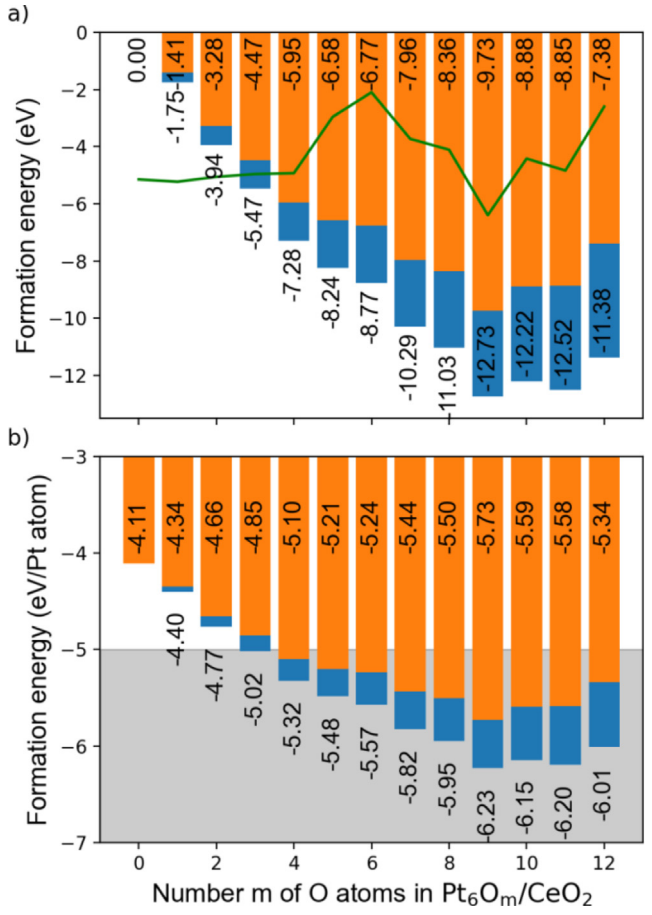

Fig. 10. a) Calculated formation energies of ceria-supported Pt_6O_m clusters taking the reduced ceria-supported Pt_6 cluster and free O_2 molecules as references, i.e. according to the reaction: $Pt_6/CeO_2 + m(½O_2) \rightarrow Pt_6O_m/CeO_2$, m = 0–12. The green line shows adhesion (deposition) energies of Pt_6O_m on $CeO_2(1\,1\,1)$, according to the reaction: $Pt_6O_m + CeO_2 \rightarrow Pt_6O_m/CeO_2$. b) Calculated formation energies of the ceria-supported Pt_6O_m clusters per Pt atom taking gas-phase Pt atoms, the $CeO_2(1\,1\,1)$ surface, and O_2 as references, i.e. according to the reaction: $6Pt + CeO_2 + m(½O_2) \rightarrow Pt_6O_m/CeO_2$. These values represent the energy gain, per Pt atom, of forming a Pt_6O_m cluster, which can be directly compared to the adsorption energies (from −5.0 to −7.3 eV, grey-shaded area) of strongly bound Pt^{2+} cations on (1 0 0)-like facets of ceria [55,68,69]. Blue bars are DFT energies ΔE at 0 K; orange bars are Gibbs free energies ΔG corresponding to conditions of the present experiments, temperature 300 K and O_2 pressure 0.01 atm (1 vol% O_2). (For interpretation of the references to color in this figure legend, the reader is referred to the web version of this article.)

Fig. 10b illustrates the energy gain per Pt atom of forming a $Pt_6O_m/CeO_2(1\,1\,1)$ cluster from gas-phase Pt atoms, the $CeO_2(1\,1\,1)$ surface, and gas-phase O_2 (the reaction $6Pt + CeO_2 + m(½O_2) \rightarrow Pt_6O_m/CeO_2$). This allows comparing the average stability of each Pt atom to adsorption energies calculated for Pt^{2+}-SA species strongly anchored on (1 0 0)-like facets of ceria. Such adsorption energy of Pt^{2+} on O_4 sites of ceria nanoparticles and surfaces ranges from −5.0 to −7.3 eV [55,68,69], indicated by the shaded area in Fig. 10b. According to these energies the stability of Pt atoms is similar in the PtO_x clusters and the Pt^{2+}-SA species. This explains why the oxidation of metallic Pt clusters on ceria upon exposure to O_2 can result in both dispersed Pt^{2+}-SA species and PtO_x clusters. However, since the re-dispersion of Pt clusters as the Pt^{2+}-SA species requires relatively scarce surface O_4 sites, the formation of PtO_x clusters is more likely, especially for catalysts with high Pt loadings.

Details on the evolution of the structure and atomic charges of Pt_6O_m clusters supported on $CeO_2(1\,1\,1)$ for m = 0 to 12 are given in the Supplementary Material. O atoms on the supported Pt_6O_m clusters preferentially adsorb in bridge sites of Pt-Pt bonds formed by the least electron-depleted Pt atoms and break the bonds by creating quasi-linear -O-Pt-O- fragments. The consecutive addition of O atoms increases the Bader charge of the involved Pt atoms until reaching ca. 1.2 |e| (see Fig. S12) in the Pt_6O_9/CeO_2 system, where all Pt-Pt bonds are transformed into Pt-O-Pt ones. This system is the most stable with respect to oxygen content variations and also corresponds to the most strongly anchored particle (see adhesion energies in Fig. 10a), suggesting its lower volatility compared to other Pt_6O_m clusters. The predominant structural motif in these oxidized PtO_x clusters is that of d^8 Pt(II) complexes, with Pt cations in a square-planar coordination environment bonded to four O anions.

Regarding the catalytic properties of these systems, it should be noted both CO and O_2 interact strongly with bare metallic Pt clusters, with an almost barrier-less dissociation of molecular O_2 [70]. However, the low-temperature oxidation of CO on metallic Pt clusters is hindered by poisoning with CO, which is adsorbed 0.1 – 0.3 eV more strongly than O_2 [71], thus blocking adsorption (and dissociation) of the latter. Elevated temperatures are required to reduce the CO coverage on metallic Pt, make the adsorption of O_2 possible, and thus facilitate CO oxidation. In turn, CO adsorption on atomically dispersed Pt^{2+} species seems to depend on the ceria support, with either very weak (calculated adsorption energy of −0.1 [68], 0.1 [71] and 0.2 eV [55]) or moderate (calculated adsorption energy of 0.8–0.9 eV [29]) bonding. The weak bonding is hardly sufficient for noticeable CO surface residence even at sub-ambient temperatures, and the moderate bonding was associated with a quite high activation barrier of 0.8–0.9 eV for the rate-limiting O_2 dissociation step [29].

On the Pt_6O_9/CeO_2 model, we have identified two CO adsorption modes. The first contains molecular CO bound to a Pt atom in a terminal way by 0.5–0.8 eV (upper panels in Fig. S13). The second adsorption mode features CO_2– or CO_3-like moieties bound by 1.5–2.1 eV with respect to free CO plus Pt_6O_9/CeO_2 (lower panels in Fig. S13). CO_2 desorption from these structures resulting in Pt_6O_8/CeO_2 requires as little as 0.2–0.5 eV and is energetically favored with respect to free CO plus Pt_6O_9/CeO_2 by over 1.5 eV. Such nearly spontaneous CO_2 formation is due to the strongly activated CO forming one or two extra O-CO bonds with the oxidized PtO_x clusters. These computational findings shed light on the role of ceria-supported oxidized PtO_x clusters in the observed CO oxidation activity at sub-ambient temperatures. A forthcoming in-depth DFT study of the multiple mechanisms is required to elucidate details of the catalytic activity of these systems. Such study will also address low-temperature CO oxidation mechanisms beyond those proposed for Au-containing catalysts [72] or the Pt_8O_{14}/

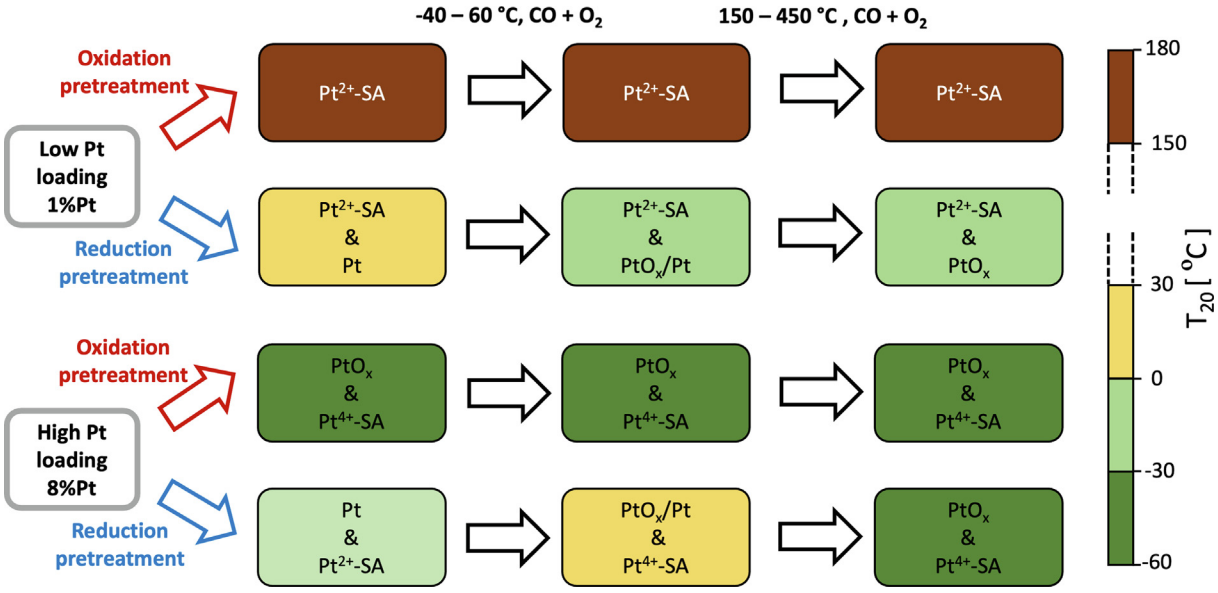

Fig. 11. Scheme summarizing the nature and activity of Pt species in Pt/CeO_2 catalysts as a function of Pt content (low 1 wt% Pt; high 8 wt% Pt), pretreatment, and exposure to CO oxidation conditions at low (-40 to 60 °C) and high (150 to 450 °C) temperature. Majority Pt species are mentioned inside each box, whose background is colored according to the temperature at which 20% CO conversion is reached (T_{20}). Pt^{2+}-SA refers to atomically dispersed Pt^{2+} species, i.e. Pt^{2+}-O_4, which for low Pt loadings are found mainly in surface positions of ceria. For high Pt loadings Pt^{2+}-SA and Pt^{4+}-SA species also occupy bulk-like positions in ceria under reducing and oxidizing conditions, respectively. Pt refers to metallic Pt, either in the form of particles or clusters, and PtO_x/Pt refers to partially oxidized Pt particles where a fraction of Pt-Pt bonds still preserved. PtO_x refers to fully oxidized Pt particles or clusters without Pt-Pt bonds.

CeO_2 model [29], the latter of which already provided an explanation of more facile CO oxidation over PtO_x particles than Pt^{2+}-SA species.

We also note that the adsorption energy of CO on the reduced Pt_6/CeO_2 system (2.45 eV) is comparable to those calculated for the Pt_6O_9/CeO_2 system. Interaction with CO therefore does not significantly destabilize PtO_x clusters with respect to Pt clusters. The DFT data discussed in this section thus explain the transformations between different states of ceria-supported Pt catalysts under varying conditions, and describe the stability and chemical properties of the states involved in these transformations.

4. Conclusions

This work addressed the redox properties and performance of Pt/CeO_2 catalysts that are highly active towards the oxidation of CO at sub-ambient temperatures, even below 0 °C. We demonstrate how Pt-loading, pre-treatments, and exposure to reaction conditions affect the structure, oxidation state, and resulting activity of these catalysts, as schematically summarized in Fig. 11.

Depending on the Pt loading, oxidative and reductive pre-treatments of the catalyst samples have opposite effects on their low-temperature CO oxidation activity. For catalysts with high Pt content (8%Pt and 15%Pt), pre-oxidation enhanced the activity more than pre-reduction. In turn, the reductive pre-treatment enhanced the activity of the catalyst with low Pt loading (1%Pt) more significantly. However, pre-reduced catalysts for all Pt loadings were further transformed after exposure to the CO + O_2 reaction medium, with activities surpassing those of the corresponding pre-oxidized catalysts.

These trends in the activity can be traced back to changes in the nuclearity and oxidation states of the Pt species, as revealed by *in situ* and *ex situ* XPS. In the pre-oxidized $1Pt/CeO_2$ catalyst, platinum mainly forms Pt^{2+} single atoms. This state is highly stable and active in the CO oxidation only at T > 100 °C via a MvK mechanism involving O atoms from CeO_2. Pre-oxidized catalysts with high Pt loadings, in turn, contain platinum as Pt^{2+} and Pt^{4+} cations, forming PtO_x particles. The latter trigger the CO oxidation activity below 0 °C, involving CO and oxygen adsorbed directly on the PtO_x particles. Pre-treatment of the catalysts in H_2 leads to the presence of both Pt^{2+} and metallic Pt species (in the form of Pt clusters and nanoparticles). However, the fraction of metallic Pt is significantly lower for the catalyst with low Pt loading. Thus generated metallic Pt particles are more active at sub-ambient temperatures than the atomically dispersed Pt^{2+} species, but less active than the PtO_x species in the corresponding oxidized catalysts.

Crucially, *operando*-induced changes appear because metallic Pt particles are prone to oxidation when exposed to the CO + O_2 reaction mixture, resulting in the corresponding increase of the CO oxidative activity below 0 °C. Heating the high-loading $8Pt/CeO_2$ and $15Pt/CeO_2$ catalysts in the reaction mixture to 30 °C initiates a partial oxidation of Pt clusters with the formation of first Pt-O-Pt bonds. Finally, completely oxidized PtO_x clusters are formed at/above 350 °C, where basically all Pt-Pt bonds are transformed into Pt-O-Pt bonds. For the low-loading $1Pt/CeO_2$, the re-oxidation of the reduced catalyst in the reaction mixture mainly restores [Pt^{2+}-O_4] sites with atomically dispersed Pt atoms embedded in CeO_2, possibly accompanied by the formation of a small amount of PtO_x clusters.

Pt particles are transformed to PtO_x because these oxidized states are notably more stable, according to the formation energies of our globally optimized models calculated with DFT-based approaches. In fact, PtO_x clusters also compete in stability with the Pt^{2+}-SA species, the formation of which requires the presence of square-planar O_4 surface sites. The similar stability of Pt species and relatively low concentration of the O_4 sites can explain why PtO_x particles are the dominant species for oxidized catalysts with high Pt loadings.

To summarize, this study has demonstrated the key role of oxidized PtO_x particles for the catalytic oxidation of CO at very low temperature. Metallic Pt particles, often considered as the most active state in such catalysts, are in fact precursors for the formation, under *operando* conditions, of more active PtO_x particles. This highlights the need to understand the complex response of cat-

alytic materials to both pre-treatments and *operando* conditions in order to design catalyst preparation strategies that maximize the abundance of active species.

Data availability

The computational data that support the findings of this study are available in the Supplementary Material and in the ioChem-BD repository at doi.org/10.19061/iochem-bd-6-145.

Declaration of Competing Interest

The authors declare that they have no known competing financial interests or personal relationships that could have appeared to influence the work reported in this paper.

Acknowledgements

This work was supported by the Ministry of Science and Higher Education of the Russian Federation within the governmental order for Boreskov Institute of Catalysis (project AAAA-A21-121011390 053-4). J.Q., P.C.-L., A.B. and K.M.N. gratefully acknowledge support by the Spanish/FEDER *Ministerio de Ciencia, Innovación y Universidades* (grants PGC2018-093863-B-C22, PID2021-128217NB-I00, MDM-2017-0767 and CEX2021-001202-M) as well as by the grants of the *Generalitat de Catalunya* 2018BP00190 (for A.B.), 2021SGR00286 and 2017SGR13. A.B acknowledges the support of the Junior Leader Programme from "La Caixa Foundation". M.V. would like to thank the Czech Science Foundation for financial support under project no. 20-13573S. The TEM studies were carried out using facilities of the shared research centers: "National center of investigation of catalysts" at Boreskov Institute of Catalysis and "VTAN" at Novosibirsk State University. Computer resources have been partly provided by the Red Española de Supercomputación. This study was also supported the by European COST Actions CA18234 and CA21101. The CERIC-ERIC Consortium is acknowledged for access to NAP-XPS experimental facility and financial support.

Appendix A. Supplementary data

Supplementary data to this article can be found online at https://doi.org/10.1016/j.jcat.2023.03.004.

References

[1] J. Jansson, Low-Temperature CO Oxidation over Co_3O_4/Al_2O_3, J. Catal. 194 (2000) 55–60.
[2] Y. Lou, X.-M. Cao, J. Lan, L. Wang, Q. Dai, Y. Guo, J. Ma, Z. Zhao, Y. Guo, P. Hu, G. Lu, Ultralow-temperature CO oxidation on an In_2O_3-Co_3O_4 catalyst: a strategy to tune CO adsorption strength and oxygen activation simultaneously, Chem. Commun. 50 (2014) 6835–6838.
[3] X. Xie, Y. Li, Z.-Q. Liu, M. Haruta, W. Shen, Low-temperature oxidation of CO catalysed by Co_3O_4 nanorods, Nature 458 (2009) 746–749.
[4] M. Okumura, N. Masuyama, E. Konishi, S. Ichikawa, T. Akita, CO Oxidation below Room Temperature over Ir/TiO_2 Catalyst Prepared by Deposition Precipitation Method, J. Catal. 208 (2002) 485–489.
[5] T.S. Kim, J.D. Stiehl, C.T. Reeves, R.J. Meyer, C.B. Mullins, Cryogenic CO Oxidation on TiO_2-Supported Gold Nanoclusters Precovered with Atomic Oxygen, J. Am. Chem. Soc. 125 (2003) 2018–2019.
[6] X.-L. Wang, X.-P. Fu, W.-W. Wang, C. Ma, R. Si, C.-J. Jia, Effect of Structural Evolution of Gold Species Supported on Ceria in Catalyzing CO Oxidation, J. Phys. Chem. C 123 (2019) 9001–9012.
[7] M. Haruta, T. Kobayashi, H. Sano, N. Yamada, Novel Gold Catalysts for the Oxidation of Carbon Monoxide at a Temperature far Below 0 °C, Chem. Lett. 16 (1987) 405–408.
[8] S. Gatla, D. Aubert, G. Agostini, O. Mathon, S. Pascarelli, T. Lunkenbein, M.G. Willinger, H. Kaper, Room-Temperature CO Oxidation Catalyst: Low-Temperature Metal-Support Interaction between Platinum Nanoparticles and Nanosized Ceria, ACS Catal. 6 (2016) 6151–6155.
[9] E.M. Slavinskaya, A.I. Stadnichenko, V.V. Muravyov, T.Y. Kardash, E.A. Derevyannikova, V.I. Zaikovskii, O.A. Stonkus, I.N. Lapin, V.A. Svetlichnyi, A.I. Boronin, Transformation of a Pt–CeO_2 Mechanical Mixture of Pulsed-Laser-Ablated Nanoparticles to a Highly Active Catalyst for Carbon Monoxide Oxidation, ChemCatChem 10 (2018) 2232–2247.
[10] N. Imanaka, T. Masui, H. Imadzu, K. Yasuda, Carbon monoxide oxidation at room temperature on Pt/CeO_2–ZrO_2–Bi_2O_3 catalysts, Chem. Commun. 47 (2011) 11032–11034.
[11] E.M. Slavinskaya, R.V. Gulyaev, A.V. Zadesenets, O.A. Stonkus, V.I. Zaikovskii, Y. V. Shubin, S.V. Korenev, A.I. Boronin, Low-temperature CO oxidation by Pd/CeO_2 catalysts synthesized using the coprecipitation method, Appl. Catal. B: Environ. 166–167 (2015) 91–103.
[12] Y. Nagai, T. Hirabayashi, K. Dohmae, N. Takagi, T. Minami, H. Shinjoh, S. Matsumoto, Sintering inhibition mechanism of platinum supported on ceria-based oxide and Pt-oxide-support interaction, J. Catal. 242 (2006) 103–109.
[13] D. Pierre, W. Deng, M. Flytzani-Stephanopoulos, The importance of strongly bound Pt-CeO_x species for the water-gas shift reaction: Catalyst activity and stability evaluation, Top. Catal. 46 (2007) 363–373.
[14] J. Lee, Y. Ryou, X. Chan, T.J. Kim, D.H. Kim, How Pt Interacts with CeO_2 under the Reducing and Oxidizing Environments at Elevated Temperature: The Origin of Improved Thermal Stability of Pt/CeO_2 Compared to CeO_2, J. Phys. Chem. C 120 (2016) 25870–25879.
[15] J. Jones, H. Xiong, A.T. DeLaRiva, E.J. Peterson, H. Pham, S.R. Challa, G. Qi, S. Oh, M.H. Wiebenga, X.I. Pereira Hernández, Y. Wang, A.K. Datye, Thermally stable single-atom platinum-on-ceria catalysts via atom trapping, Science 353 (2016) 150–154.
[16] J. Ke, W. Zhu, Y. Jiang, R. Si, Y.-J. Wang, S.-C. Li, C. Jin, H. Liu, W.-G. Song, C.-H. Yan, Y.-W. Zhang, Strong Local Coordination Structure Effects on Subnanometer PtO_x Clusters over CeO_2 Nanowires Probed by Low-Temperature CO Oxidation, ACS Catal. 5 (2015) 5164–5173.
[17] J. Lee, Y. Ryou, J. Kim, X. Chan, T.J. Kim, D.H. Kim, Influence of the Defect Concentration of Ceria on the Pt Dispersion and the CO Oxidation Activity of Pt/CeO_2, J. Phys. Chem. C 122 (2018) 4972–4983.
[18] J.G. Nunan, H.J. Robota, M.J. Cohn, S.A. Bradley, Physicochemical properties of Ce-containing three-way catalysts and the effect of Ce on catalyst activity, J. Catal. 133 (1992) 309–324.
[19] X.I. Pereira-Hernández, A. DeLaRiva, V. Muravev, D. Kunwar, H. Xiong, B. Sudduth, M. Engelhard, L. Kovarik, E.J.M. Hensen, Y. Wang, A.K. Datye, Tuning Pt-CeO_2 interactions by high-temperature vapor-phase synthesis for improved reducibility of lattice oxygen, Nat. Commun. 10 (2019) 1358.
[20] A.M. Gänzler, M. Casapu, P. Vernoux, S. Loridant, F.J. Cadete Santos Aires, T. Epicier, B. Betz, R. Hoyer, J.-D. Grunwaldt, Tuning the Structure of Platinum Particles on Ceria In-Situ for Enhancing the Catalytic Performance of Exhaust Gas Catalysts, Angew. Chem., Int. Ed. 56 (2017) 13078-13082.
[21] A.M. Gänzler, M. Casapu, F. Maurer, H. Störmer, D. Gerthsen, G. Ferré, P. Vernoux, B. Bornmann, R. Frahm, V. Murzin, M. Nachtegaal, M. Votsmeier, J.-D. Grunwaldt, Tuning the Pt/CeO_2 Interface by in-Situ Variation of the Pt Particle Size, ACS Catal. 8 (2018) 4800–4811.
[22] K. Ding, A. Gulec, A.M. Johnson, N.M. Schweitzer, G.D. Stucky, L.D. Marks, P.C. Stair, Identification of active sites in CO oxidation and water-gas shift over supported Pt catalysts, Science 350 (2015) 189–192.
[23] A. Holmgren, F. Azarnoush, E. Fridell, Influence of pre-treatment on the low-temperature activity of Pt/ceria, Appl. Catal. B: Environ. 22 (1999) 49–61.
[24] X.I. Pereira Hernández, A.T. DeLaRiva, H. Xiong, D. Kunwar, E.J. Peterson, A.K. Datye, Y. Wang, B. Sudduth, Reversible Transformation from Pt Single Atoms to Sub-Nanometer Particles for Low Temperature CO Oxidation, AIChE Annual Meeting, Minneapolis, United States (2017) 75–78.
[25] F.C. Meunier, L. Cardenas, H. Kaper, B. Šmíd, M. Vorokhta, R. Grosjean, D. Aubert, K. Dembélé, T. Lunkenbein, Synergy between Metallic and Oxidized Pt Sites Unravelled during Room Temperature CO Oxidation on Pt/Ceria, Angew. Chem., Int. Ed. 60 (2021) 3799–3805.
[26] J. Li, Y. Tang, Y. Ma, Z. Zhang, F. Tao, Y. Qu, In Situ Formation of Isolated Bimetallic PtCe Sites of Single-Dispersed Pt on CeO_2 for Low-Temperature CO Oxidation, ACS Appl. Mater. Interfaces 10 (2018) 38134–38140.
[27] X. Hong, Y. Sun, Effect of Preparation Methods on the Performance of Pt/CeO_2 Catalysts for the Catalytic Oxidation of Carbon Monoxide, Catal. Lett. 146 (2016) 2001–2008.
[28] Q. Fu, H. Saltsburg, M. Flytzani-Stephanopoulos, Active Nonmetallic Au and Pt Species on Ceria-Based Water-Gas Shift Catalysts, Science 301 (2003) 935–938.
[29] H. Wang, J.-X. Liu, L.F. Allard, S. Lee, J. Liu, H. Li, J. Wang, J. Wang, S.H. Oh, W. Li, M. Flytzani-Stephanopoulos, M. Shen, B.R. Goldsmith, M. Yang, Surpassing the single-atom catalytic activity limit through paired Pt-O-Pt ensemble built from isolated Pt_1 atoms, Nat. Commun. 10 (2019) 3808.
[30] A.I. Boronin, E.M. Slavinskaya, A. Figueroba, A.I. Stadnichenko, T.Y. Kardash, O. A. Stonkus, E.A. Fedorova, V.V. Muravev, V.A. Svetlichnyi, A. Bruix, K.M. Neyman, CO oxidation activity of Pt/CeO_2 catalysts below 0 °C: platinum loading effects, Appl. Catal. B: Environ. 286 (2021).
[31] E.A. Derevyannikova, T.Y. Kardash, A.I. Stadnichenko, O.A. Stonkus, E.M. Slavinskaya, V.A. Svetlichnyi, A.I. Boronin, Structural Insight into Strong Pt–CeO_2 Interaction: From Single Pt Atoms to PtO_x Clusters, J. Phys. Chem. C 123 (2019) 1320–1334.
[32] S. Gatla, D. Aubert, V. Flaud, R. Grosjean, T. Lunkenbein, O. Mathon, S. Pascarelli, H. Kaper, Facile synthesis of high-surface area platinum-doped ceria for low temperature CO oxidation, Catal. Today 333 (2019) 105–112.

[33] J. El Fallah, L. Hilaire, M. Roméo, F. Le Normand, Effect of surface treatments, photon and electron impacts on the ceria 3d core level, J. Electron Spectrosc. Relat. Phenom. 73 (1995) 89–103.
[34] C.D. Wagner, W.M. Riggs, L.E. Davis, J.F. Moulder, G.E. Muilenberg, Handbook of X-ray Photoelectron Spectroscopy, Perkin-Elmer, Eden Prairie, USA, 1979.
[35] R.V. Gulyaev, A.I. Stadnichenko, E.M. Slavinskaya, A.S. Ivanova, S.V. Koscheev, A.I. Boronin, In situ preparation and investigation of Pd/CeO_2 catalysts for the low-temperature oxidation of CO, Appl. Catal. A: Gen. 439–440 (2012) 41–50.
[36] R.V. Gulyaev, E.M. Slavinskaya, S.A. Novopashin, D.V. Smovzh, A.V. Zaikovskii, D.Y. Osadchii, O.A. Bulavchenko, S.V. Korenev, A.I. Boronin, Highly active $PdCeO_x$ composite catalysts for low-temperature CO oxidation, prepared by plasma-arc synthesis, Appl. Catal. B: Environ. 147 (2014) 132–143.
[37] A.I. Stadnichenko, V.V. Murav'ev, V.A. Svetlichnyi, A.I. Boronin, Platinum state in highly active Pt/CeO_2 catalysts from the X-ray photoelectron spectroscopy data, J. Struct. Chem. 58 (2017) 1152-1159.
[38] M. Vorokhta, I. Khalakhan, M. Vondráček, D. Tomeček, M. Vorokhta, E. Marešová, J. Nováková, J. Vlček, P. Fitl, M. Novotný, P. Hozák, J. Lančok, M. Vrňata, I. Matolínová, V. Matolín, Investigation of gas sensing mechanism of SnO_2 based chemiresistor using near ambient pressure XPS, Surf. Sci. 677 (2018) 284–290.
[39] Y. Lykhach, F. Faisal, T. Skála, A. Neitzel, N. Tsud, M. Vorokhta, F. Dvořák, K. Beranová, Y. Kosto, K.C. Prince, V. Matolín, J. Libuda, Interplay between the metal-support interaction and stability in $Pt/Co_3O_4(111)$ model catalysts, J. Mater. Chem. A 6 (2018) 23078–23086.
[40] G. Kresse, J. Hafner, Ab initio molecular dynamics for liquid metals, Phys. Rev. B 47 (1993) 558-561.
[41] G. Kresse, J. Furthmuller, Efficient iterative schemes for ab initio total-energy calculations using a plane-wave basis set, Phys. Rev. B 54 (1996) 11169.
[42] J.P. Perdew, J.A. Chevary, S.H. Vosko, K.A. Jackson, M.R. Pederson, D.J. Singh, C. Fiolhais, Atoms, molecules, solids, and surfaces: Applications of the generalized gradient approximation for exchange and correlation, Phys. Rev. B 46 (1992) 6671-6687.
[43] J.P. Perdew, J.A. Chevary, S.H. Vosko, K.A. Jackson, M.R. Pederson, D.J. Singh, C. Fiolhais, Erratum: Atoms, molecules, solids, and surfaces: Applications of the generalized gradient approximation for exchange and correlation, Phys. Rev. B 48 (1993) 4978-4978.
[44] V.I. Anisimov, F. Aryasetiawan, A.I. Lichtenstein, First-principles calculations of the electronic structure and spectra of strongly correlated systems: the LDA + U method, J. Phys.: Condens. Matter 9 (1997) 767.
[45] A. Migani, G.N. Vayssilov, S.T. Bromley, F. Illas, K.M. Neyman, Dramatic reduction of the oxygen vacancy formation energy in ceria particles: a possible key to their remarkable reactivity at the nanoscale, J. Mater. Chem. 20 (2010) 10535–10546.
[46] G.N. Vayssilov, Y. Lykhach, A. Migani, T. Staudt, G.P. Petrova, N. Tsud, T. Skála, A. Bruix, F. Illas, K.C. Prince, V. Matolín, K.M. Neyman, J. Libuda,, Support nanostructure boosts oxygen transfer to catalytically active platinum nanoparticles, Nat. Mater. 10 (2011) 310–315.
[47] C. Loschen, J. Carrasco, K.M. Neyman, F. Illas, First-principles LDA+U and GGA +U study of cerium oxides: Dependence on the effective U parameter, Phys. Rev. B 75 (2007).
[48] P.E. Blöchl, Projector augmented-wave method, Phys. Rev. B 50 (1994) 17953.
[49] M.K. Bisbo, B. Hammer, Efficient Global Structure Optimization with a Machine-Learned Surrogate Model, Phys. Rev. Lett. 124 (2020).
[50] J.E.Q. Domínguez, K.M. Neyman, A. Bruix, Stability of oxidized states of freestanding and ceria-supported PtOx particles, J. Chem. Phys. 157 (2022).
[51] J. Rogal, K. Reuter, Ab Initio Atomistic Thermodynamics for Surfaces: A Primer. Exp. Model. Simul. Gas-Surf. Interact. React. Flows Hypersonic Flights, 2006, 2–1 – 2–18.
[52] K. Reuter, Ab Initio Thermodynamics and First-Principles Microkinetics for Surface Catalysis, Catal. Lett. 146 (2016) 541–563.
[53] A. Jan, J. Shin, J. Ahn, S. Yang, K.J. Yoon, J.-W. Son, H. Kim, J.-H. Lee, H.-I. Ji, Promotion of Pt/CeO_2 catalyst by hydrogen treatment for low-temperature CO oxidation, RSC Adv. 9 (2019) 27002–27012.
[54] L.R. Borges, A.G.M. da Silva, A.H. Braga, L.M. Rossi, M.A. Suller Garcia, P. Vidinha, Towards the Effect of $Pt^0/Pt^{\delta+}$ and Ce^{3+} Species at the Surface of CeO_2 Crystals: Understanding the Nature of the Interactions under CO Oxidation Conditions, ChemCatChem 13 (2021) 1340–1354.
[55] A. Bruix, Y. Lykhach, I. Matolínová, A. Neitzel, T. Skála, N. Tsud, M. Vorokhta, V. Stetsovych, K. Ševčíková, J. Mysliveček, R. Fiala, M. Václavů, K.C. Prince, S. Bruyère, V. Potin, F. Illas, V. Matolín, J. Libuda, K.M. Neyman, Maximum Noble-Metal Efficiency in Catalytic Materials: Atomically Dispersed Surface Platinum, Angew. Chem., Int. Ed. 53 (2014) 10525-10530.
[56] F. Maurer, J. Jelic, J. Wang, A. Gänzler, P. Dolcet, C. Wöll, Y. Wang, F. Studt, M. Casapu, J.-D. Grunwaldt, Tracking the formation, fate and consequence for catalytic activity of Pt single sites on CeO_2, Nat. Catal. (2020).
[57] M.S. Hegde, P. Bera, Noble metal ion substituted CeO_2 catalysts: Electronic interaction between noble metal ions and CeO_2 lattice, Catal. Today 253 (2015) 40–50.
[58] R. Fiala, M. Vaclavu, A. Rednyk, I. Khalakhan, M. Vorokhta, J. Lavkova, V. Potin, I. Matolinova, V. Matolin, Pt–CeO_x thin film catalysts for PEMFC, Catal. Today 240 (2015) 236–241.
[59] https://xpssimplified.com/elements/platinum.php.
[60] Y. Lykhach, S.M. Kozlov, T. Skála, A. Tovt, V. Stetsovych, N. Tsud, F. Dvořák, V. Johánek, A. Neitzel, J. Mysliveček, S. Fabris, V. Matolín, K.M. Neyman, J. Libuda, Counting electrons on supported nanoparticles, Nat. Mater. 15 (2016) 284–288.
[61] P. Dolcet, F. Maurer, M. Casapu, J.-D. Grunwaldt, Insights into the Structural Dynamics of Pt/CeO_2 Single-Site Catalysts during CO Oxidation, Catalysts 11 (2021) 617.
[62] Y.S. Kim, A. Bostwick, E. Rotenberg, P.N. Ross, S.C. Hong, B.S. Mun, The study of oxygen molecules on Pt (111) surface with high resolution x-ray photoemission spectroscopy, J. Chem. Phys. 133 (2010).
[63] A. Bruix, J.A. Rodriguez, P.J. Ramírez, S.D. Senanayake, J. Evans, J.B. Park, D. Stacchiola, P. Liu, J. Hrbek, F. Illas, A New Type of Strong Metal-Support Interaction and the Production of H_2 through the Transformation of Water on $Pt/CeO_2(111)$ and $Pt/CeO_x/TiO_2(110)$ Catalysts, J. Am. Chem. Soc. 134 (2012) 8968–8974.
[64] L. Bianchettin, A. Baraldi, S.d. Gironcoli, E. Vesselli, S. Lizzit, L. Petaccia, G. Comelli, R. Rosei,, Core level shifts of undercoordinated Pt atoms, J. Chem. Phys. 128 (2008).
[65] D.R. Mullins, K.Z. Zhang, Metal-support interactions between Pt and thin film cerium oxide, Surf. Sci. 513 (2002) 163–173.
[66] A.D. Allian, K. Takanabe, K.L. Fujdala, X. Hao, T.J. Truex, J. Cai, C. Buda, M. Neurock, E. Iglesia, Chemisorption of CO and Mechanism of CO Oxidation on Supported Platinum Nanoclusters, J. Am. Chem. Soc. 133 (2011) 4498–4517.
[67] A. Beniya, S. Higashi, Towards dense single-atom catalysts for future automotive applications, Nat. Catal. 2 (2019) 590–602.
[68] N. Daelman, M. Capdevila-Cortada, N. López, Dynamic charge and oxidation state of Pt/CeO_2 single-atom catalysts, Nat. Mater. 18 (2019) 1215–1221.
[69] X. Wang, J.A. van Bokhoven, D. Palagin, Atomically dispersed platinum on low index and stepped ceria surfaces: phase diagrams and stability analysis, Phys. Chem. Chem. Phys. 22 (2020) 28–38.
[70] P.C. Jennings, H.A. Aleksandrov, K.M. Neyman, R.L. Johnston, A DFT study of oxygen dissociation on platinum based nanoparticles, Nanoscale 6 (2014) 1153–1165.
[71] H.A. Aleksandrov, K.M. Neyman, K.I. Hadjiivanov, G.N. Vayssilov, Can the state of platinum species be unambiguously determined by the stretching frequency of an adsorbed CO probe molecule?, Phys Chem. Chem. Phys. 18 (2016) 22108–22121.
[72] W. Dononelli, L.V. Moskaleva, T. Klüner, CO Oxidation over Unsupported Group 11 Metal Catalysts: New Mechanistic Insight from First-Principles, J. Phys. Chem. C 123 (2019) 7818–7830.